Aus der Klinik und Poliklinik für Orthopädie und Unfallchirurgie

Direktor: Universitätsprofessor Dr. med. P. Eysel

Aus dem Schwerpunkt Unfall -, Hand – und Ellenbogenchirurgie

Leiter: Universitätsprofessor Dr. med. L. – P. Müller

Detailed anatomy of the ventral and lateral part of the elbow joint capsule and its influence on the elbow stability

Inaugural-Dissertation zur Erlangung der Doktorwürde

der Medizinischen Fakultät

der Universität zu Köln

vorgelegt von

Xintong Chen

Aus Hunan(P.R.China)

promoviert am 03. August 2023

Dekan: Universitätsprofessor Dr. med. G. R. Fink

1. Gutachter: Professor Dr. med. K. Wegmann

2. Gutachterin: Professorin Dr. rer. nat. F. Pröls

3. Gutachter: Privatdozent Dr. med. D. Akgün

<u>Erklärung</u>

Ich erkläre hiermit, dass ich die vorliegende Dissertationsschrift ohne unzulässige Hilfe Dritter und ohne Benutzung anderer als der angegebenen Hilfsmittel angefertigt habe; die aus fremden Quellen direkt oder indirekt übernommenen Gedanken sind als solche kenntlich gemacht.[1]

Bei der Auswahl und Auswertung des Materials sowie bei der Herstellung des Manuskripteshabe ich Unterstutzung von folgenden Personen erhalten:

......Univ.Prof. Dr. med. L. – P. Müller.....................
......Prof. Dr. med. Kilian Wegmann.............................
..... Stephanie Kahmann..

Weitere Personen waren an der geistigen Herstellung der vorliegenden Arbeit nicht beteiligt. Insbesondere habe ich nicht die Hilfe einer Promotionsberaterin/eines Promotionsberaters in Anspruch genommen. Dritte haben von mir weder unmittelbar noch mittelbar geldwerte Leistungen für Arbeiten erhalten, die im Zusammenhang mit dem Inhalt der vorgelegten Dissertationsschrift stehen.

Die Dissertationsschrift wurde von mir bisher weder im Inland noch im Ausland in gleicher oder ähnlicher Form einer anderen Prüfungsbehörde vorgelegt.

Erklärung zur guten wissenschaftlichen Praxis:

Ich erkläre hiermit, dass ich die Ordnung zur Sicherung guter wissenschaftlicher Praxis und zum Umgang mit wissenschaftlichem Fehlverhalten (Amtliche Mitteilung der Universität zu Köln AM 24/2011) der Universität zu Köln gelesen habe und verpflichte mich hiermit, die dort genannten Vorgaben bei allen wissenschaftlichen Tätigkeiten zu beachten und umzusetzen.

Köln, den 10.10.2023   Unterschrift:

Die dieser Arbeit zugrunde liegenden Experimente sind von mir mit Unterstützung von Herrn Prof. Dr. med. Kilian Wegmann und den wissenschaftliche Mitarbeiterin Frau Stephanie Kahmann durchgeführt worden.

Die Proben für diesen Versuch wurden vom Anatomie-Labor an der Medizinischen Universität Graz   zur Verfügung gestellt.

Die Erhebung und Auswertung der experimentellen Daten sowie die statistische Analysesowie bei der Herstellung des Manuskriptes wurden von mir selbst durchgeführt.

Univ.Prof. Dr. med. L. – P. Müller und Prof. Dr. med. Kilian Wegmann liefert Ideen für experimentelle Programmdesigns.

Frau Stephanie Kahmann führte mich durch den technischen Teil des Experiments und die Übersetzung der deutschen Zusammenfassung.

Acknowledgements

The completion of a doctoral dissertation not only requires a lot of my own efforts, but also cannot do without the support of others. So here I would like to express my gratitude to those who have helped me.

The first one I want to say thanks is my supervisor Prof. Dr. med. Kilian Wegmann. It was he who helped me find the exact research goal.

The next one is Stephanie Kahman, For me she is more than a good partner, but also a good friend. She is a patient and loving person. Without her encouragement and understanding, it would have been very difficult for me to successfully complete my dissertation.

I would also like to thank Prof. Dr. Andreas Weiglein at Medizinische Universitaet Graz, who provided great help with my experimental materials. Although he passed away now, I wish his family all the best.

Finally, I would like to thank my husband. Without his care for me in life, without his tolerance for me, it would be difficult for me to persist in completing my work.

In addition, I would like to thank all the friends and partners I met while living and working in Germany. May they all accomplish their life goals

Index

Glossary

AL   annular ligament

ALL   anterior longitudinal ligament

CAD   computer-aided design

CCD   charge coupled device

CEI   complex elbow instability

CIP   computer image processing

CMOS   complementary metal oxide semiconductor

CT   computed tomography

DF   Dynamic Fluoroscopy

DP   digital photoelasticity

DIC   digital image correlation

Fig   figure

FEA   fnite element analysis

LCL   later collateral ligament

LUCL   lateral ulnar collateral ligament

MCL   medial collateral ligament

aMCL   anterior bundle of the medial collateral ligament

7

pMCL   posterior bundle of the medial collateral ligament

MUCL   medial ulnar collateral ligament

pMUCL   posterior bundle of medial ulnar collateral ligament

PLRI   posterolateral rotatory instability

PMRI   posteromedial rotatory instability

UCL   ulnar collateral ligament

Tab   table

RCL   radial collateral ligament

ROI   regions of interest

FPRT   forearm pronation resistance test

Introduction

1. Background

The elbow joint is among the most matched joints in the human body. It comprises of the humerus in the lower part, and the ulna and the radius in the upper part. It includes three joints, namely the ulno-humeral, theradio-humeral joint, and the proximal radio-ulnar joint. As the joint between the shoulder and wrist, it plays a vital role in movement and functions of the upper extremity. It not only expands the range of motion of the hand but also provides power, accuracy, and stability for hand movement [1]. The elbow joint enables flexion movement in addition to the combined motion of pronation and supination at the same time, the elbow joint is the only joint in the human body to provide this varying function [2].

Maintaining the normal function of the human elbow joint depends greatly on stability. Instability may occur due to trauma, for example when the hand is extended when a person falls over, and laxity may present due to repetitive external rotation forces, such as that observed in athletes who throw frequently [3]. Treating elbow instability requires knowledge about the roles that the various structures within the joint contribute, especially in relation to providing stability. The anatomical features of the elbow reveal intrinsic bone stability and a variety of essential soft tissue stabilizers, these features are the present focus of research. The soft tissue stabilizers include the anterior and posterior joint capsules, the surrounding muscles, and the medial and lateral collateral ligament-complexes. Since some ligaments cannot be clearly distinguished from the joint capsule, this structure is referred to as the capsule complex. Compared to other structures in the body, the studies pertaining to the elbow capsule are still in preliminary stages and need to be explored further. Tyrdal and Olsen[4] ascertained that the pathophysiology relating to elbow joint injuries is closely related to the destruction of the joint capsule. Differentiating and distinguishing the contributions of each of the different parts of the joint capsule in relation to elbow stability has important theoretical implications and practical

applications.

2. Research Advances

2.1. Advancement of Elbow Instability Studies

2.1.1. Anatomy of the Elbow Joint

The anatomical structure that maintains the elbow joint stability includes bones, ligaments, joint capsules, and muscle tissue. When any part of this structure is damaged, elbow joint instability occurs. Clinically, this is more common in cases of elbow dislocation, deformity, and ulnar dislocation. After the bone, ligament, or joint capsule of the elbow joint has been damaged, the incidence of recurrent dislocation and chronic instability or osteoarthritis increases. When characterized in accordance to the importance of maintaining stability, these anatomical structures fall into two categories: the first group includes the humeral-ulnar joint, the lateral ulnar collateral ligament (LUCL), and the anterior bundle of the medial collateral ligament (aMCL); the second group includes the radial head, articular capsule, flexor muscle group and the extensor muscle group. Although these two groups of structures maintain the stability of the elbow joints together, the first group of structures is normally considered to be more critical. When structures of the first group are damaged, the second group of structures can play a compensatory and stabilising role [5].

Ligaments

The elbow joint ligaments consist of both medial and lateral collateral ligament-complexes. The lateral collateral ligament-complex (LCL-complex) consists of an annular ligament (AL), a lateral ulnar collateral ligament (LUCL), and a radial collateral ligament (RCL). The AL and the ulnar notch wrap together around the humeral head to maintain the humeral head's stability in the superior elbow joint during the rotational movement of the forearm. It is an important limitation in the proximal radio-ulnar joint, and even more so in pediatric elbow instability. The RCL is a thick and nearly triangular fibrous tissue originating from the humerus' external

epicondyle, ending at the radial notch and the ulna's AL. Moreover, the LUCL terminates posterior to the AL from the lateral epicondyle of humerus along the supinator crest of ulna [6]. The RCL gradually merges with the AL, and together they maintain the humeral head's stability. In contrast, the LUCL is primarily responsible for preventing postero-lateral dislocation and precluding varus of the elbow joint. If the LUCL is damaged, surgical repair may be required [7, 8].
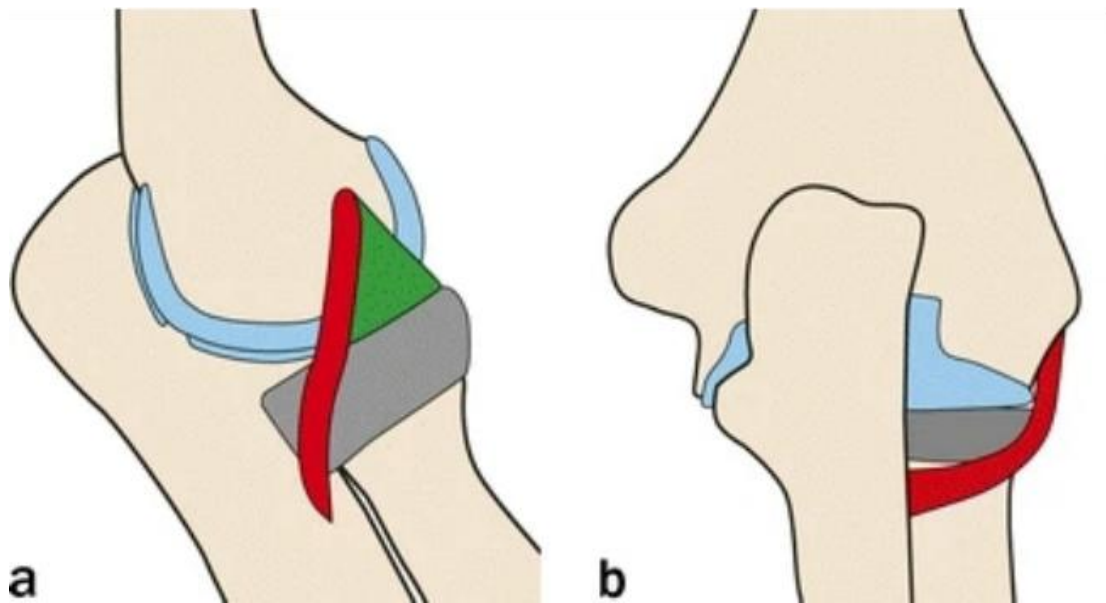
Fig. 1 Anatomy of the LCL-complex [9]

a Diagrammatic representation of the LCL-complex. The RCL (green) is sector-shaped and is fused with fibers in the AL (grey). The LUCL (red) is extended from the lateral epicondyle on the posterior aspect of the radius over the superior crest of the ulna. b Back view of the LCL, LUCL (red) surrounds the radial head to form a suspensory.

The medial collateral ligament-complex (MCL-complex) is the most crucial stabilizing structure used to prevent valgus, and the anterior bundle plays the most important role in this process. We also describe this as the ulnar collateral ligament (UCL/MUCL). It is composed of three interconnected independent ligaments, the anterior, posterior and transverse bundles. The anterior bundle (aMCL) originates in front of the medial epicondyle of the humerus and ends in a minor nodule on the inner

margin of the coronoid process, slightly fan-shaped. The posterior bundle(pMCL) begins behind the medial epicondyle of the humerus and terminates on the bone surface of the inner edge of the olecranon. Its fibers are fan-shaped. The transverse bundle is thinner and extends from the medial epicondyle of the humerus and fuses with the aMCL and the pMCL at the coronal process and olecranon via transverse or oblique bundles [10]. During elbow flexion and extension, the aMCL and pMCL play synergistic roles: when the elbow is straightened, the aMCL is tense whereas the pMCL is relaxed; when the elbow is flexed, the aMCL is relaxed, and the pMCL tenses. Biomechanical studies [11] have shown that the MCL-complex is a stable and critical structure preventing valgus in elbow flexion from 20°~120°, and the aMCL is the most important structure within the MCL complex. The posterior insertion provides a greater contribution towards stability in higher degrees of elbow flexion [12].
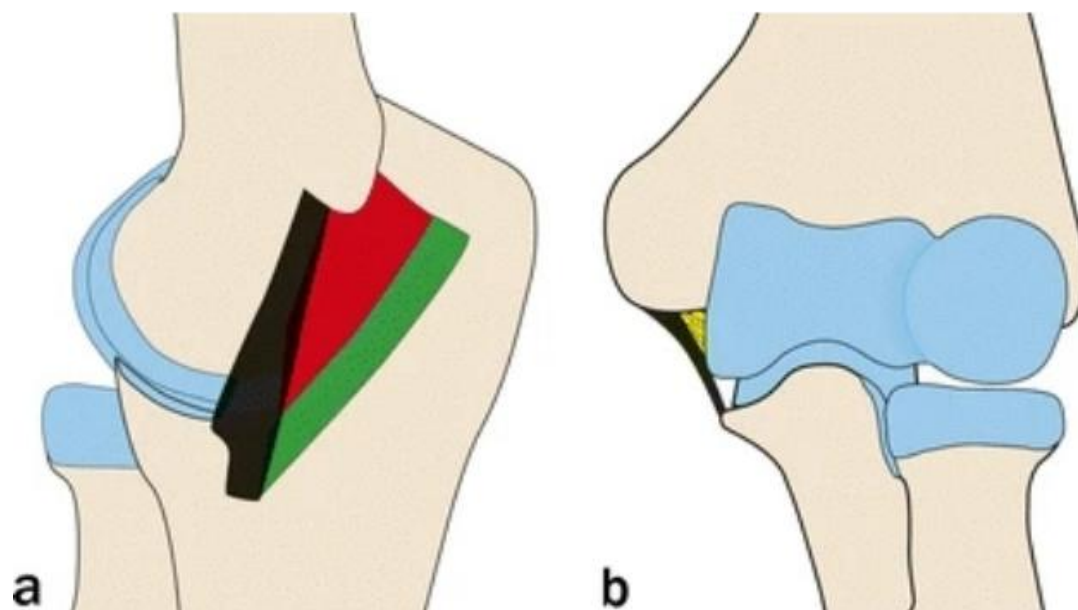
Fig. 2 Anatomy of the MCL-complex [9]

a Diagrammatic representation of the MCL. The aMCL (black) is a coagulation of a slightly more concentrated joint capsule, while the pMCL (red) seems rather triangular. Both of these structures begin on the inferior surface of the medial epicondyle. The green part is the transverse ligament. b Anterior view of the elbow joint. The common MCL sits aligned with the sublime tubercle of the ulna. There is

generally a tiny intra-articular fat pad (yellow) below the fibers of the MCL.

<u>Bones</u>

Since the elbow is a compound joint, three separate joints are encased in one communal joint capsule: the humeral-ulnar joint, the humeral-radial joint, and the proximal radial-ulnar joint [13].

The humeral-ulnar joint is the foremost bony stable structure of the elbow joint. During elbow flexion, the tip of the ulnar coronoid process matches with humeral coronoid fossa; during elbow extension, the tip of ulnar olecranon matches with humeral olecranon fossa; when the elbow is in a neutral position, the middle of ulnar incisura trochlearis matches with humeral trochlear groove. Only 7.5° valgus and a 5.3° rotational range of motion were found in the humeral-ulnar joint [14]. Furthermore, there is a lateral angle of 10-20° between the ulna and the humerus, which is called the valgus carrying angle of the elbow [15]. Given that most of the elbow joint pressure is transmitted between the coronoid process and the humeral trochlear, the coronoid process of the ulna is a crucial component of this joint. In general, the relationship between the coronoid process and elbow stability is classified by the size of its broken fragments [16]. Former research indicates that this consists of an anterior projection and an anteromedial facet (AMF), which together form the coronoid process. The anterior projection is the anterior support of the elbow joint and leads to severe instability when the injury rate is > 25% [17, 18, 19]. Concomitantly, as the AMF is a medial proximal elongation of the ulna, it is susceptible to fracture when opposing varus rotation forces are applied [20, 21]. In contrast, the loss of the olecranon leads to development of severe elbow instability only when it reaches >75% [22]. Thus, clinically, we often choose the tip of the ipsilateral/contralateral olecranon as a graft for treating coronoid process fractures [23, 24]. These special anatomical features provide the elbow joint with an inherent stability against varus and valgus forces. The humerus-ulnar joint was shown to provide 55% of the anti-valgus stabilization and during elbow extension, and 75% of

the anti-valgus stabilization during elbow flexion [25].

The humerus-radial joint is the second most important stabilizing structure of the elbow joint against valgus. As the mainstay of this, the most considerable role of the radial head is to avoid the occurrence of elbow valgus deformity during periods of growth and development. In the adult, valgus and pronation of the radial head is the second constraint applied to the collateral ligament, which can provide 20% to 30% valgus stability [25]. Hall's [26] clinical studies confirmed that the kinematic changes of the elbow increased its relaxation following a radius head defect, and the posterior subluxation of the proximal radius stump aggravated instability of the elbow joint. Schneeberger [27] reported that with a complete lateral collateral ligament, the posterolateral rotation relaxation degree increased by 9.6°following removal of the radius head. The stability of the radial head was recovered incompletely after radial head replacement. These studies have confirmed the contribution of the radial head in relation to stability. However, it was mentioned earlier that the MCL complex serves as the strongest stabilizing structure in combatting valgus stress. If the MCL-complex is broken, and the radius head of the fracture is also absent, this will lead to severe instability of the elbow joint. Therefore, the radius head should not be resected when radius head fracture is accompanied by damage to the MCL-complex. Besides these functions, the humerus-radial joint also plays a role in conductive stress. The distal radius carries most of the wrist stress, 60% of which continues to be transmitted through the humerus-radial joint, and the remaining 40% is transmitted to the ulna through the lower ulnar-radial joint and the interosseous membrane [28].

<u>Muscles</u>

There are four groups of muscles around the elbow joint: anterior, posterior, lateral and medial. The anterior muscle group includes the biceps brachii and brachial muscle; the posterior muscle group consists of the triceps and elbow muscle; the lateral muscle group includes the extensor muscle of wrist and hand, the supinator, and the brachioradialis muscle; whilst the medial muscle group is composed of the palmaris teres, pronator longus, and the flexors muscle of the hands and wrists.

During elbow joint movement, the synergy of the elbow muscles plays a dynamic stabilizing role. In particular, the anconeus muscle, which originates from the external palate and is widely connected to the ulna, is one of the necessary factors in countering instability of the posterolateral rotation [29, 30, 31].

Capsules

A fibrous articular capsule covers the entire elbow joint. The weakness of posterior and anterior joint capsules is strengthened by the medial and lateral collateral ligament complexes on both sides. There are several fat pads between the fibro-articular capsule and the synovial membrane. The elevation and displacement of these fat pads may indicate the existence of elbow instability.

Traditionally, we only differentiate the joint capsule regions using general terms such as the anterior and posterior parts. Lee M. Reiche [32] further subdivided the anterior and posterior joint capsules into six parts by identifying six distinct bands. The anterior lateral band originates on the distal humerus's anterolateral aspect in close proximity to the lateral supracondylar ridge, and its distal end inserts at the anterior superior AL. The anterior medial oblique band begins at the anteromedial aspect of the elbow joint, which is the lateral portion of the superior border of the medial humeral condyle, and extends into the anterior central and medial AL laterally and distally. The anterior transverse band is composed of transverse-type course fibers that insert from the medial aspect of the trochlear superior ridge to the anterior medial AL on a medial superior side to the lateral inferior side. The posterior transverse band crosses the olecranon fossa transversally from the medial to the lateral edge of the olecranon fossa above, and the inferior ends at the medial and lateral posterior trochlear ridges. The two remaining bands at the posterior capsule are opposite to each other and form an angle. Posterior medial oblique band originates at the posterior ridge of the medial trochlear and the posterior lateral oblique band originates at the posterior ridge of the lateral trochlear, respectively ending above the sides of the olecranon tip. These latter three bands form an inverted triangular shape.

The anterior capsule is tense when the elbow joint is stretched and the posterior

capsule is tense when the elbow joint is flexed [33]. In addition the capsule and ligament fuse at the joint. Biomechanical studies have shown that when the elbow joint is in a straight state, the entire capsule can resist 70% tension, 38% valgus stress, and 32% varus stress; whereas the capsule can resist 13% valgus stress and 8% varus stress when the elbow joint is in a 90° flexion position [25]. Previously it was thought that although the joint capsule has a positive effect on maintaining elbow joint stability, a role is only played by the articular capsule when the bone and ligament structures are damaged at the same time. Therefore, it is frequently assumed that the joint capsule can be completely removed as long as the bone and ligament structures are intact in elbow stiffness patients [34]. This perspective refers only to the joint capsule treatment under specific conditions. There have been experiments dedicated to understanding the stability provided by the elbow capsule; however, these sources of literature are relatively old [35, 36, 37]. Based on the important roles that joint capsules play in other joints, we can assume that these previous studies were insufficient. Japanese scholars [38] found there is a substantial attachment of the elbow joint's anterior capsule on the radial side of the coronoid process. They predicted there may be a correlation between the thick attachment of the capsule and the stability of the humeral joint. In 2018, a study by Edwards showed that there are specific areas on the posterior joint capsule that are attached to the capitulum, which is important elbow stability and it should be defined as the Osborne-Cotterill ligament [39].

2.1.2. Classification of Elbow Instability

A comprehensive assessment of elbow instability is necessary prior to definitive diagnosis and rational classification.

In 2000, O'Driscoll [40] classified instability according to five criteria:

① The timing (acute, chronic, or recurrent)

② The articulation(s) involved (elbow versus radial head)

③ The direction of displacement (valgus, varus, anterior, posterolateral

rotatory)

④   The degree of displacement (subluxation or dislocation)

⑤   The presence or absence of associated fractures

Surveys have shown that at least 26% of elbow dislocations are associated with fractures [41]. These forms of instability accompanied by fractures are usually referred to as complex elbow instability (CEI) [42]. Tarassoli [43], proposed that under these conditions, injuries should be divided into four main categories: "1. Transolecranon fracture dislocation, 2. Elbow dislocation with concomitant fracture of the coronoid, 3. Elbow dislocation in the presence of the radial head fracture, and 4. Elbow dislocation with coronoid and radial head fracture (the terrible triad)." This taxonomy covers almost all of the features of the injuries and is very comprehensive and concise. It has also been suggested that using the Wrightington classification system to manage elbow dislocations is more helpful in differentiating the mechanism of injury and for guiding treatment [44]. Wrightington categorized elbow dislocations with fractures into six subtypes based on the engagement of the coronoid and the radial head: [45]

"A.   Anteromedial facet fracture;

B.   Bifacet fracture;

B+.   Bifacet fracture and radial head fracture;

C.   Comminuted radial head or combined radial head and anterolateral facet;

D.   Diaphyseal proximal ulna fracture with dislocated intact radial head;

D+.   Diaphyseal proximal ulna fracture and radial head fracture. "

Either way, this classification reflects the fact that various research groups have been working continuously in the area of elbow instability, and exploring and studying its pathogenesis.

2.1.3. Pathological Mechanism

Elbow joint stability is usually divided into two categories, dynamic stability and static stability. The former is dependent on the bone structure of the elbow joint and

the surrounding ligaments and joint capsules, while the latter is contingent on the muscles around the joint. Trauma and degeneration are the most direct causes of elbow instability. Studies have shown that the elbow joint is second only to the shoulder joint in incidence number of all dislocations [46, 47].

Valgus Instability

Valgus instability is commonly seen in patients with chronic strain injuries, most of whom seek medical attention due to symptoms relating to ulnar nerve excitation. However, valgus instability can also be seen in acute injuries. Acute valgus instability mainly occurs in patients with elbow dislocations due to tears in the anterior bundle of the MCL, and is usually accompanied by other soft tissue injuries. Such instability is often seen during the forearm pronation resistance test (FPRT) following dislocation correction. Most acute anterior bundle injuries can self-heal and rarely cause recurrent elbow instability. However, acute anterior MCL injury caused by pronation and torsion force exerted on the elbow joint, for example in throwing athletes, are difficult to heal without reasonable and effective treatment [48]. It triggers lateral column compression and elbow joint loosening in the valgus, which together may develop into chronic elbow pronation instability.

Varus Instability

The presence of the elbow's valgus carrying angle predisposes the elbow to valgus instability, while individual varus instability is rare. In addition, the tension force acts on the lateral elbow joint for longer time, especially when the varus stress passes through the elbow joint, therefore lateral ligament injury is more prone to the sequelae of joint relaxation than the medial ligament injury [49]. Furthermore, some research groups have reported that a dysfunction of the lateral collateral ligament of the elbow joint may be secondary to repeated glucocorticoid injections in some patients [50]. Extensive surgical removal treating the external humeral epicondylitis would weaken the lateral ligament function, leading to varus instability of the elbow [51].

Posterolateral Rotatory Instability (PLRI)

PLRI is the most prevalent type of elbow instabilities. It is also the modality most commonly responsible for recurrent elbow instability [40]. The most common elbow posterior dislocation mechanism is the posterolateral rotational injury mechanism presented by O'Driscoll et al [52]. This type of injury is common when people fall with their palm impacting on the ground. Under these circumstances the elbow joint is slightly flexed; the elbow joint is simultaneously subjected to axial, external rotation, and valgus stress, and the joint capsule and ligament ring stabilization structure around the elbow joint are damaged from the outside to the inside, eventually leading to posterior dislocation of elbow joint. According to the injury process, the dislocation of the elbow joint can be divided into three steps: step I: the ulnar beam of LCL is damaged, resulting in instability of the posterior lateral rotation, and in step II, the anterior and posterior joint capsules are further damaged, and the elbow joint is posteriorly subluxated. Step III consists of steps IIIa and IIIb. In step IIIa, the ligaments, and joint capsules are completely damaged except for the anterior MCL, and the elbow joint continues to dislocate posteriorly. During step IIIb, all of the ligaments and joint capsules are damaged, and there is a complete loss of stability relating to varus/valgus and rotation.

In addition to the PLRI steps and injuries, iatrogenic injuries of the LUCL should also be highlighted. When treating tennis elbow extensor tendon lysis and radius head resection, the LUCL is often injured by mistake and this leads to posterolateral rotation instability.

Posteromedial Rotatory Instability (PMRI)

Traditionally, PMRI is thought to be caused by fractures of the anteromedial coronal plane and associated injuries of the LUCL [53, 54, 55]. As already discussed, the posterior bundle of the medial collateral ligament (pMCL) is an essential adjunctive stabilizer, preventing posterior medial instability of the elbow in coronoid defects. Once the coronoid has been injured, increased average forearm internal rotation and articular incoordination after pMCL is cut [56]. In situations where non-fixable

coronoid fractures occur, such as defects exceeding 50% of coronoid height, the pMCL affords the main stability structure, and some stability can be restored with graft reconstruction in 90° flexion of the elbow joint [57]. There are also studies [58] that have shown that an isolated transection of the pMCL can lead to PMRI, represented by an abnormal gap that can be found between the proximal end of the ulnar-humeral joint of the medial elbow. Importantly, restoration of the joint gap after pMCL repair also proved its importance [59].

Anterior Instability

Anterior elbow instability is relatively uncommon, accounting for only 0-2.6% of all elbow instability cases [60]. As the structures on the frontal side elbow joint are stronger, anterior dislocation requires more force to occur and is usually accompanied by fractures and neurovascular injury. This is therefore generally classified as a complex dislocation. Hyperextension is the primary mechanism of injury. Most cases of anterior instability were recorded as secondary to tears in the MCL or LCL and anterior dislocation of the elbow joint after an olecranon fracture. Treatment is mainly aimed at the fractures, in rare cases at secondary problems in chronic anterior instability [61].

2.2. Experimental Methods in Biomechanics

Biomechanics is a subdiscipline of biophysics that studies the motion and deformation of living organisms. It is an emerging edge discipline formed by the intersection and interpenetration of various disciplines, mainly through mechanical principles and methods to understand the laws of life processes, and aims to solve scientific problems in the field of life and health sciences. Orthopaedic biomechanics is the most common branch of biomechanics, and focuses on the locomotor system. This type of research is often performed by testing and measuring the mechanical parameters of the bones, skeletal muscles, tendons and ligaments, joints, the spine, and other skeletal muscular systems in order to comprehensively evaluate the

specimen. With the development of computer technology, orthopaedic research methods have gradually shifted towards computerized local image simulation and extensive numerical analysis, resulting in a new branch of the discipline called computational biomechanics, which has raised the development of clinical orthopaedics to a new peak.

We have searched through the published information and propose that the following test methods are the most commonly used in orthopaedic biomechanics.

2.2.1. Electronic Universal Testing Machine

In biomechanical studies, the electronic universal testing machine is the most widely used and also the earliest method employed. Because of its direct test logic, it has not been replaced to date [62]. At the core of this approach is a loading system which simulates the various motion conditions that biological tissues might be exposed to, such as tensile, compressive or, bending forces, torsion, pure shear, pull-out, and torque tests. People capture the changes in the specimen with their bare eyes or by using other sensors. After some data processing, the relationship between the perceived mechanical changes and the loading system is produced as readable results. For example, the crest value force and stiffness (measured as a linear gradient) can be withdrawn from force-displacement graph as produced by the material testing system. Thereafter the marker data can be analyzed and the tissue strain can be calculated using motion analysis software or other techniques. Although this method is primitive, it can be accurately combined with a digital tracking system to monitor changes in motion. So it is often used as a component alongside other experimental methods [62].

2.2.2. Electrical Strain Gauge Technology (ESGT)

Whether it is a mechanical study of bone, soft tissue or other materials, ESGT can be used to measure small deformations on the surface of samples. The main principle of this method is that a minor strain on the surface of a measured sample causes a minor deformation in the resistive wire on the surface of the resistive sheet, which results in

a minor change in electrical resistance. This electrical change is amplified and transformed into a strain value according to the set ratio. Some researchers have analyzed the linearity error, temperature effect error, and magnetic field effect error in ESGT and have reduced these errors using the differential bridge and half-bridge. This is a good foundation for the biomechanical test results to become closer to reality [63]. The ESGT method has a number of advantages, such as high measurement accuracy, simple and easy-to-use strain gauges, and a wide range of applications (model tests, solid tests, static tests, and dynamic tests), consequently it is used in a variety of mechanical tests. However, the ESGT method exhibits a number of shortcomings. It can only measure the average linear deformation of each test point on the surface of the sample when the entire sample stress change needs to be measured, therefore plenty of test points must be taken on the surface of the sample, and the workload is relatively large. It also cannot determine the local strain peak of stress concentration with a high degree of accuracy [64].

2.2.3. Photoelasticity Method

The photoelastic method focuses on the stress distribution of the sample. Anisotropic transparent crystals are inherently birefringence, this is called the Permanently Birefringence. The anisotropic transparent non-crystalline sample does not have this property, however, when stress is applied to this material, it shows anisotropic properties, resulting in a temporary birefringence phenomenon. The photoelastic method uses photosensitive materials with Temporary Birefringence properties to obtain a stress photogram consisting of black-white or colored stripes, whilst also applying an external load with polarized light. The stress photogram can then be calculated and analyzed to acquire the stress-strain situation both on the surface and on the inside of the measured sample [65]. Since the 1980s, the digital photoelasticity method has been continuously developed. It consists of the automatic acquisition and processing of photoelastic parameters and the automation of sample stress analysis. The digital photoelasticity method has great potential in many areas, including

real-time crack analysis, dynamic stress analysis, and anisotropic materials damage investigations. This method is still under development and needs more research [66]. In the 1980s, Digital Photoelasticity (DP) was introduced. This research method combines computer-aided design (CAD) and computer image processing (CIP) techniques with photoelasticity. It includes the automatic acquisition and processing of photoelastic parameters, combined with the automation of sample stress analysis. DP has great potential for development in several aspects of interest, including real-time crack and dynamic stress analysis, and for studying damage in anisotropic materials [66].

2.2.4. Pressure Sensitive Film Method

The pressure sensitive film method seems simple and does not require large pieces of equipment, but it still requires sophisticated digital image analysis software to process the information on the film [67]. As the elbow joint consists of three joints, the film can be placed on the joint surface between two of them, and the pressure measured between the joint surfaces under different conditions, thus indirectly inferring joint stability from the results [68]. However, as mentioned previously, the elbow joint is not a weight-bearing joint. The correlation between joint stability and contact pressure is not as obvious as the lower limbs. Moreover, the material properties of the film itself make the accuracy of the measurements questionable. The texture of the film is different from cartilage which can affect joint activity, and the results are also relatively dependent on the environmental situation [69, 70]. Placing the film on the articular surface requires the joint to be opened, which would destroy the integrity of the articular capsule. This obviously does not facilitate our exploration of the joint capsule.

2.2.5. Ultrasound Elastographic Assessment

Ultrasound elastographic assessment is based on the premise that the speed of sound transmission in a solid medium is significantly greater than in air and that the speed of

sound transmission in a solid medium is associated with the elastic properties and density of the solid. (Ultrasound elastography assessment of bone/soft tissue interface) The sound propagation speed is therefore measured, and the modulus of elasticity of the solid is calculated via a formula. The advantages of ultrasound include the ability to provide high-resolution images of soft tissue, a lack of radiation exposure, it is easy to access and low cost, the technique is non-destructive, and has other advantageous qualities besides these. It is also easier to perform dynamic examinations in comparison to other radiological examinations [71, 72]. It is possible to visually see changes in thickness in the various parts of the elbow joint capsule during movements due to the force. The relative stiffness of the joint capsule can be expressed in terms of the strain rate, which is determined as the ratio of the strain in the joint capsule to the strain in the acoustic coupler [73]. High-resolution ultrasound can also detect the direction of soft tissue fibers. Without doing histological testing, ultrasounds can be used to get a general idea of the directional trend of the fibers.

However, ultrasound testing relies heavily on skilled technicians. When sample sizes are relatively large, the data processing efficiency is very low. It is also important to note that the test method does not have a direct measurement of sound intensity, consequently the scanning acoustic microscope scale is generally used to indirectly measure the speeds of the sound waves [74].

2.2.6. Intracapsular Pressure Monitoring

Intracapsular pressure monitoring is a biomechanical study modality utilized for capsular tissue only. It provides a continuous response to changes in the elasticity and compliance of the capsule wall. Intracapsular pressure is typically measured using a Touhy needle, which is inserted into a closed, nonvolume-consuming space, and is connected to a pressure transducer, which then forms an invasive pressure monitoring device [75]. As a result, pressure changes can be monitored by gradually injecting saline, and pressure values can also be observed under different positions. However, because intracapsular pressure monitoring is an invasive detection method, it causes damage to the integrity of the tissue. Therefore, it does not

perfectly reflect the biomechanical properties of the capsule wall, and there is some inaccuracy involved. More importantly, it is not possible to partition in order to determine the mechanical properties of the individual capsule parts.

2.2.7. Computerized 3D Image Reconstruction and the Finite Element Analysis (FEA).

Currently, human specimens are in short supply for the purposes of orthopaedic biomechanical testing. The advantages of combining computerized 3D image reconstruction and FEA are that it can reduce the amount of required human cadaver tests and also detect the interaction mechanisms between each part of the human specimen.

The computerized 3D image reconstruction technique can compensate for the problems observed in the previous biomechanical testing methods, which were limited to measuring changes in mechanical properties on the surface of the sample and could not involve or determine the interaction of the parts within the sample under mechanical action [76]. Moreover, the application of this technique within clinical settings is relatively established [77]. However, an inadequacy pertaining to computer 3D reconstruction is that the accuracy is not presently great enough to meet experimental requirements.

The FEA method is a simulation test; the shortcoming of this technique is that the accuracy of the finite element model depends on the number of selected units. Therefore, the requirement for the establishment of the finite element model is relatively high [78].

2.2.8. Dynamic Fluoroscopy System (DF) Combined with Computed Tomography (CT)

CT segmentations of each bone are usually used to create 3D reconstructions. Landmarks can be identified on 3D reconstructions of each bone and used to define

subject-specific anatomical coordinate systems. An experimental can track the trajectory after aligning its bony mark with the DFdevice. This device can be used to measure the displacement of a point between the two bones of a joint during exercise. We use a small displacement to refer to the high joint stability value roughly [79, 80]. The DF + CT method refers to a clinical study. With a real person in sports, the fixation is poor, but auxiliary CT can improve the accuracy. There are predecessors who used the DF system and tested the inclination angle (α) of the lesser sigmoid notch to study the biomechanical characteristics of the elbow stability [81].

Despite the clear advantages of this system, this method does not make full use of the specimen. Specimens that have been destroyed can no longer be used in other tests. Therefore, the number of specimens is relatively high. Besides these technical problems, this method also delivers some radiation damage to the experimenter.

2.2.9. Electronic Speckle Pattern Interferometry (ESPI)

The principle of ESPI is that when a laser beam is irradiated onto the rough surface of a sample, the diffused light caused by the diffuse reflection forms interference and generates a random distribution of light-dark spots. Deformation of the sample is derived by measuring the amplitude of the light wave of the object in the image plane after imaging through the lenses. It is suitable for measuring the in/off-plane displacement of solid surfaces. This method is advantageous due to its high accuracy, non-contact processing, low vibration isolation requirements, as well as its ability to display interference fringes in real-time. The associated disadvantages are that operation of the technique is manual, and the workload associated with it is large. In recent years, an improved method based on the traditional scattering interferometry technique combined with computer and digital image processing techniques has been proposed [82], which provides the advantages of high sensitivity alongside acquisition of the full 3D displacement [83].

There are too many other methods to mention, however the methods listed above are generally regarded as unsuitable for the research we are focusing on. There are

also some limitations of conditions that cannot be rectified or achieved. Given these caveats and limitations, digital image correlation (DIC) was selected as the most appropriate method overall.

2.3. Digital Image Correlation (DIC)

DIC is an image measurement method which applies computer vision technology. It has the advantageous characteristics of being non-interference, non-contact, non-destructive, and available for full-field morphology, displacement and deformation measurements, and additionally benefits from its low experimental environment requirements, strong anti-interference ability and simple light path [84, 85]. DIC techniques were first proposed in 1982 by Peters in the U.S and Yamaguchi et al. in Japan [86, 87]. In recent decades, with the deepening of theoretical research and the gradual improvement of testing systems by scholars from various countries, as well as the rapid development of digital cameras and computer technology, DIC technologies have been applied increasingly widely in civil engineering, experimental mechanics, materials science, aerospace, and life sciences.

2.3.1. DIC Measurement System

The DIC measurement system mainly consists of two parts: hardware (test loading equipment, image acquisition equipment and computer) and a software system (correlation algorithm). (Fig. 3)
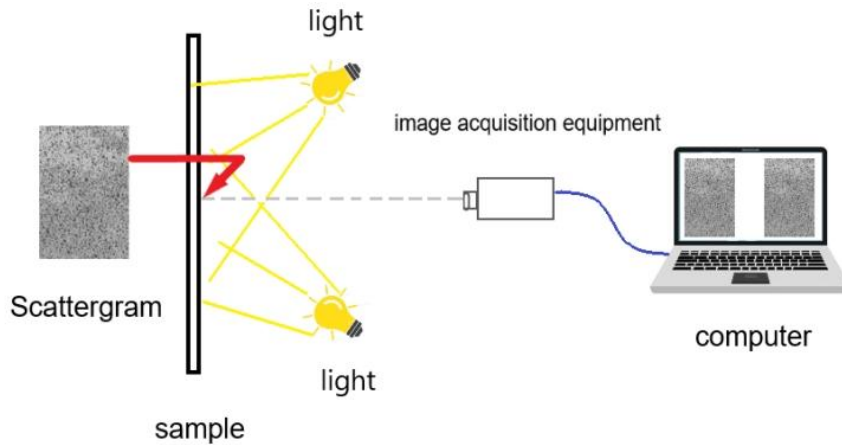
Fig. 3 DIC measurement system

Sample placed in front of image device, connected to computer. Cameras capture and send surface images for deformation analysis. Computer controls system, processes data, and delivers results. Software analyzes experiment images for deformation data.

As shown in Fig. 3, the sample is placed directly in front of the image acquisition device, which is connected to the computer.

The image acquisition equipment generally adopts CCD or CMOS cameras, which are responsible for capturing images of object surfaces and sending them to the computer as deformation information for processing; the computer is used to control the matching image acquisition system. This method gives the final result after processing and calculating the acquired image information; the software system obtains the required deformation field information by comparing and analyzing the scattered images collected throughout the experiment and then it calculates the processed information [88].

Initially, the method measures the in-plane displacement and deformation of the object being measured using a single camera, i.e., the two-dimensional digital image correlation method（2D-DIC）. However, this method necessitates an approximately flat sample surface which is perpendicular to the optical axis of the camera. Without these requirements, a specific systematic error is produced, which is very inconvenient in practice and of course the system cannot measure off-plane displacement and deformation. As a solution to these problems, researchers in the

1990's proposed a three-dimensional digital image correlation method (3D-DIC) [89, 90]. 3D-DIC uses two or more cameras. In practice, the cameras need to be calibrated on the basis of the binocular vision principle first. Then the DIC method is used to match the images acquired by the left and right hand side cameras during the motion or deformation of the object being tested. Finally, the displacement and strain data are analyzed via 3D reconstruction based on the calibration results. In comparison with the 2D-DIC method, the 3D-DIC achieves a more accurate determination of the deformation and shape of samples on curved surfaces, which greatly expands the application scope of the digital image correlation method.

2.3.2. DIC Principle

Digital image correlation methods deal with images that record the situation before, during, and after deformation. The image taken prior to deformation is usually called the "original image", and the images captured during and after deformation are called the "deformed images". The basic principle of the digital image correlation method is to locate the matching points on the "original image" and the "deformed image" [91]. A rectangular region centered on a point to be found in the original image is obtained. $F(x,y)$ represents the grey value of this point, while $G(x,y)$ represents the grey value of the point on the deformation image. The software calculates the rectangular area in the original image and the rectangular area in the deformed image using a particular related algorithm. The pixel point with the highest correlation with the original image's $F(x,y)$ point is the target point that matches the original image (x,y). This methodology enables location of the deformed position of the original pixel. Comparing both positions enables calculation of the displacement and therefore the strain can be derived.

2.3.3. Application of the Digital Image Correlation Method in Biomechanics

The digital image correlation method can easily be applied to many kinds of

mechanical properties tests of biological tissue materials, whether they are soft or hard, to obtain the displacement and strain fields of object deformation. Due to its advantageous qualities, this methodology is gradually being applied to various areas of biomechanics.

Zhang [92] selected freshly slaughtered bovine vessels and sprayed a fast-drying aerosol onto their surfaces surface to create a randomly distributed scatter field. During the loading process, the scatter images at the corresponding moments were recorded. The deformation of vascular surfaces was obtained by analyzing the scatter images using a digital image correlation method. In addition, the stress-strain curves of the vessels were obtained via stress results measured during the experiments.

A cadaveric specimen study by Maria LR [93] used DIC to describe the strain density distribution within the anterior longitudinal ligament (ALL) during both flexion and extension. The researchers compared the strains in the ALL and within specific regions of interest (ROI) of the intervertebral discs in front of the vertebral body, and the nonlinear correlations between the surface strain and the rotational and resultant moments were analyzed.

DIC is being used progressively more frequently in biomechanics. Whether its use is in orthopaedic or other subjects, it is a valuable tool for understanding pathological mechanisms in depth.

2.3.4. Selection of Specific Indicators

In summary, the DIC method is convenient and straightforward, can directly measure object displacement and deformation, has few artificial factors affecting analysis, and offers objective and accurate results. It is also a very promising method for calculating strain fields, which is widely used in the field of biomechanics. At present, there is no published literature relating to the application of digital image correlation methods for studying elbow joint capsules. It was, however, identified as the preferred solution for our study.

Displacement and strain field are both important indicators of DIC, the strain

field is computed by deriving data from the displacement for the facets. Therefore the measurement of the strain field for samples with irregular surfaces is less reliable [94, 95]. We only used the displacement field to represent the mechanical changes observed on the surfaces of the samples.

3. Research Purpose

Our objectives were to study the elbow capsule's biomechanical properties, determine its influences on elbow joint stability, and identify the most important parts of the capsule in relation to stability maintenance during various positions of the joint. This information enables better surgical access and surgical approaches, and an improved refixation method can be determined.

Materials and Methods

1. Preliminary Image Analysis of Changes in 3 Views of the Elbow Joint Capsule during Flexion and Extension Movements via the DIC.

1.1. Material

1.1.1. Specimen and Pattern Preparation

We used seven formalin-embalmed specimens of the elbow (Provided by the Anatomy Laboratory in the Medical University of Graz). All of the muscles and appendages were removed, leaving only the lower part of the humerus and the upper part of the ulna and the connected intact elbow joint capsule tissue. In order to utilise DIC for making measurements on the capsule, a high comparison black-on-white spot pattern should be prepared [95, 96]. Even though Barranger et al. applied the pattern as a powder on metal, the characteristics of biological soft tissue and the amplitude of the movements had to be taken into consideration, therefore we decided to use spray paint. A high-contrast paint was applied with a spray can, a uniform white paint base color was initially created, black paint was then used to generate black spots on top of the base colour. (Fig. 4)

Fig. 4 Prepared elbow joint specimen

On the surface of the elbow joint capsule, we first applied white paint as a base color, and then

evenly sprayed black paint spots

1.1.2. Elbow Joint Specimen Fixing Device

A metal stand was used to support the specimen, the stand comprised of a base, an upright supporting rod, a cross-connecting rod, and two screw clamps. Adjustable screws were used to hold the humerus and to adjust the position, height, and angle of specimen placement.

In addition, a protractor was printed out on an A4 piece of paper which elated to the size of the elbow, which was laminated to make it more stable and to help prevent contamination. The following steps were carried out to adjust the position of the protractor:

a) The paper protractor was hung on the cross-connecting rod. The plane was parallel to the elbow joint rotation plane.

b) The observer's line of sight was perpendicular to the protractor plane and the center of rotation of the joint coincident was aligned with the center of the protractor.

c) In the same way as b), the humerus was aligned with the 0° mark on the protractor. The observer was therefore able to make a preliminary judgment of the

angle of joint flexion and extension.

1.1.3. The DIC System

To undertake the measurements, a complete commercial 3D-DIC system (Q-400-3D, DIC, LIMESS Messtechnik und Software GmbH, Krefeld, Germany) with two video cameras (accuracy 0.01 pixel; resolution 2542 x 2052 pixel) and a light source (Brenner Import- und Großhandels Gmbh, 26W 225mA 230V 50Hz 5000K)(Fig. 5) were configured.

The images were computed using commercially available software (Istra 4D V4.4.4, LIMESS Messtechnik und Software GmbH, Krefeld, Germany).

1.2. Method

1.2.1. Recording

The distal humerus was fixed using the screw clamp on the fixation device. As described above, the rotation plane, the observer's plane of vision, and the protractor plane were kept parallel to each other. The plane being measured and the center of the joint were aligned with the lenses, and the two lenses and the joint center were kept at the same horizontal heights. Furthermore, the angle between the two lenses was maintained at between 45°and 60°, and the vertical distance between the two lenses was between 40 and 50 cm. The light source was placed on the side of the lens so that the light source was directed towards the specimen, ensuring there was not a dead angle and the line of sight of the cameras was not blocked. (Fig. 5)
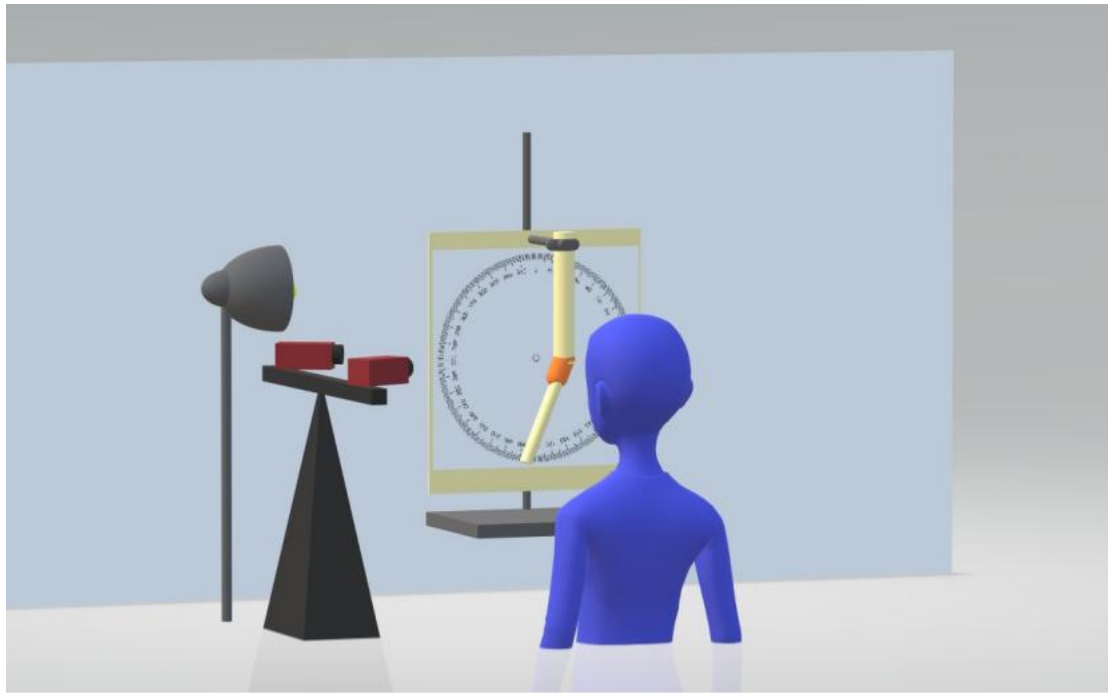
Fig. 5 Schematic diagram

The distal humerus was clamped securely. The rotation plane, observer's line of sight, and protractor plane remained parallel. The plane under measurement and joint center aligned with the lenses, all maintained at the same horizontal level. Lens angle set between 45° and 60°, with a vertical separation of 40-50 cm.

After connecting each device, the software was activated. Once the images from the two cameras were displayed on the screen, the focus of both cameras was adjusted and the image acquisition rate for each camera was set to 5 frames per second. Prior to each recording run, the commercial calibration target, a black and white porcelain card system to register the two cameras to each other automatically, was utilized.

The humerus of the specimen was secured in place using the metal stand, and the observer held the distal end of the elbow joint to flex and extend it manually at a slow and constant speed. The observer moved the arm at a frequency of 1°/s, with the specimen motionless for 5 seconds at every 10° increment.

The experiment was split into three subsets based on view, these consisted of a ventral, medial dorsal, and lateral dorsal view. The ventral view focused on the ventral part of the capsule, ranging from the middle of the humerus to the middle of the

radius and ulna. The medial dorsal view and the lateral dorsal view focus on the medial and lateral sides of the olecranon respectively, both were covered by the capsule.

The flexion angle ranges focused on were 30° to -10° for the ventral view and 50° to 140° for the medial and lateral views. Given these factors, the recording times were therefore set to 60s and 130s, resulting in 300 and 600 frames of raw data, respectively. The imaged were then sorted to identify recurring and/or noisy images, and a relationship between frame and angle was derived:(Tab. 1).

Tab. 1 Correspondence between picture and angle

	Flexion angle /(°)				
	30°	20°	10°	0°	-10°
E01					
Steps	0	42	103	150	180
E02					
Steps	0	77	137	199	282
E03					
Steps	0	76	137	190	253
E04					
Steps	0	67	128	183	240
E05					
Steps	0	55	107	179	239
E06					
Steps	0	86	133	184	240
E07					
Steps	0	60	131	198	230

The ventral view

	Flexion angle /(°)									
	50°	60°	70°	80°	90°	100°	110°	120°	130°	140°
E01										
Steps	--	--	--	--	--	--	--	--	--	--
E02										
Steps	0	60	115	164	204	254	307	367	423	--
E03										
Steps	0	70	142	221	279	332	399	447	501	--
E04										
Steps	0	58	122	172	225	267	319	362	417	--
E05										
Steps	0	59	113	172	266	325	395	438	474	--
E06										
Steps	0	56	90	138	173	214	253	290	344	--
E07										
Steps	0	45	87	131	196	236	289	345	397	--

The medial dorsal view

	Flexion angle /(°)									
	50°	60°	70°	80°	90°	100°	110°	120°	130°	140°
E01										
Steps	--	--	--	--	--	--	--	--	--	--
E02										
Steps	0	47	109	165	227	272	328	379	433	--
E03										
Steps	0	67	125	185	237	280	340	412	462	526
E04										
Steps	0	62	125	179	203	285	330	369	420	--
E05										
Steps	0	31	74	110	143	196	235	286	327	337
E06										
Steps	0	55	110	167	224	286	330	386	457	495
E07										
Steps	0	550	105	156	194	238	276	303	348	388

The lateral dorsal view

1.2.2. Evaluation ＆ Calculation of the Strain Field

Many parameters have to be adjusted to ensure appropriate conditions in order to ultimately reach the optimal outcomes when employing this multifunctional measurement technique. The values allocated to those parameters ensure that precision, accuracy, and spatial resolution are established. Due to the differing camera angles and capsule anatomical shapes within each specimen, no uniform optimal parameter standard could be employed. Therefore the parameters had to be adjusted individually for each specimen and each subset of views [97].

<u>Parameters for DIC Evaluation</u>

Evaluation of the digital image correlation was performed using the following parameters (Fig. 6).

Fig. 6 Parameter setting interface

The facet size describes the edge length of a squared subset of pixels, which accounted for one gridpoint. During our evaluations, the best coverage of the region of interest (ROI) was achieved with facet sizes of between 15 and 27 pixels. The evaluations were always performed for two image levels as recommended by the start point search. The low outlier tolerance discared fewer points and allows for a more accurate evaluation. The abort criteria was set to 0.1 pixels in the accuracy of facet identification, a maximum of 35 grey values, and a deviation of 0.8 pixels between the correlation result and the projection on the object for each facet. The grid spacing was set to 3-5 pixels, ensuring that for every 3 pixels the center of a grid point was set. In line with the 17 pixels facet size, the strong overlap allowed for a high spatial resolution. The location and orientation of the facets were determined in reference to the first camera.

To further improve the evaluation results, the start point search conditions were also set manually. Initiating at the manually set start point, each following one was searched, within a radius of 25 pixels, in increments of 5 pixels. If the properties of the start point were below one-quarter of the allowed correlation criteria (factor 0.25), the search was stopped, and the starting point was identified.

The optimal settings for each case were determined to be as follows:(Tab. 2-4).

Tab. 2 Parameter settings for the ventral view

	E01	E02	E03	E04	E05	E06	E07
Facet size/ (Pixels)	19	19	27	19	19	27	19
Image levels	two	two	two	two	two	two	two
Outlier Tolerance	low	low	Medium	low	low	low	low
Accuracy/(Pixels)	0.1	0.1	0.2	0.1	0.2	0.1	0.1
Residuum/(Grey values)	35	35	35	35	35	35	35
3D Residuum (Pixels)	0.8	0.8	0.8	0.9	0.9	0.9	0.9
Grid spacing (Pixels)	3	3	3	3	3	3	3
Reference	camera _pos_1	camera _pos_1	camera _pos_1	camera _pos_1	camera _pos_1	camera _pos_2	camera_ pos_1
Search radius (Pixels)	128	128	25	128	128	128	128
Step search radius (Pixels)	2	2	5	3	3	3	3
Stop criterion	0.25	0.25	0.25	0.25	0.25	0.25	0.25

Tab. 3 Parameter settings for the medial dorsal view

	E01	E02	E03	E04	E05	E06	E07
Facet size (Pixels)	--	29	25	19	19	17	19
Image levels	--	two	two	two	two	two	two
Outlier tolerance	--	medium	medium	low	low	low	low
Accuracy /(Pixels)	--	0.2	0.1	0.1	0.1	0.1	0.2
Residuum /(Grey values)	--	35	20	20	20	35	35
3D Residuum/(Pixels)	--	0.6	1	0.8	0.4	0.8	1
Grid spacing (Pixels)	--	5	5	3	3	4	3
Reference	--	camera_pos_1	camera_pos_1	camera_pos_1	camera_pos_1	camera_pos_2	camera_pos_1
Search radius (Pixels)	--	128	128	128	128	128	128
Step search radius (Pixels)	--	2	3	2	2	2	2
Stop criterion	--	0.25	0.25	0.25	0.25	0.25	0.25

Tab. 4 Parameter settings for the lateral dorsal view

	E01	E02	E03	E04	E05	E06	E07
Facet size (Pixels)	19	19	19	17	17	17	21
Image levels	two	two	two	two	two	two	two
Outlier tolerance	low	low	low	low	low	low	low
Accuracy (Pixels)	0.1	0.1	0.2	0.2	0.1	0.2	0.2
Residuum (Grey values)	20	20	20	35	20	35	35
3D Residuum (Pixels)	0.8	1	1	0.8	0.4	0.8	0.8
Grid spacing (Pixels)	3	3	3	3	3	3	3
Reference	camera_pos_1	camera_pos_1	camera_pos_1	camera_pos_1	camera_pos_1	camera_pos_2	camera_pos_1
Search radius (Pixels)	128	128	128	25	128	128	25
Step search radius (Pixels)	2	2	2	5	2	2	2
Stop criterion	0.25	0.25	0.25	0.25	0.25	0.25	0.25

Evaluation

The principle of the DIC method is to compare the changes of each determinable point between the reference image and the serial target images to evaluate overall deformation. In this project, the range of flexion angles for elbow joint motion was set

from plus 30° to minus 10° when studying the ventral joint capsule. Actually, there are two states of both flexion and extension. The initial image is in the state of elbow flexion which is why there are wrinkles, and the surface of the joint capsule is not fully revealed. If the first frame is set as the reference frame, the area in which the surface can be evaluated is greatly reduced. In light of this, a reverse order method was adopted which started the evaluation from the last frame in hyperextension and the image with the capsule best visible (0°) was set as the reference. Similarly, this method was adopted for the other two subsets of views.

2. Depth Analysis of the Ventral V-shaped Region of the Elbow Joint Capsule

Following the evaluation of the data, the calculated and measured displacements were interpreted. After observation of the deformation maps of all of the specimens at all of the angles, there was a distinct area of interest on the ventral side of the joint capsule. In the image, this area showed color changes which were different from the surrounding areas, thus suggesting a different deformation pattern. After considering the anatomical structure of the ventral side of the joint capsule, we proposed that the "V-shaped area" should be investigated further.

2.1. Method

2.1.1. Anatomical Positioning

The "V-shaped area" investigations were undertaken separately. Based on the obvious and generally identifiable anatomical envelope bands on the specimens and regarding Lee's [32] study, the boundaries of the v area were set out as follows: (Fig. 7).

V: Consisted of the lateral band and the anterior medial band. The lateral band originates on the distal humerus's anterolateral aspect in close proximity to the lateral supracondylar ridge and its distal end inserts at the anterior superior AL. The medial band begins at the anteromedial aspect of the elbow joint, which is the lateral portion

of the superior border of the medial humeral condyle, and extends into the anterior central and medial AL laterally and distally.

1 area: The triangular area between the above two bands.

2 area: The area beyond the anterior lateral band and within the anterior medial oblique band.

Fig. 7 Division diagram

*V: Two bands. **1** : The triangular area between the above two bands. **2** : The area beyond the anterior lateral band and within the anterior medial oblique band*

2.1.2. Setting the ROI

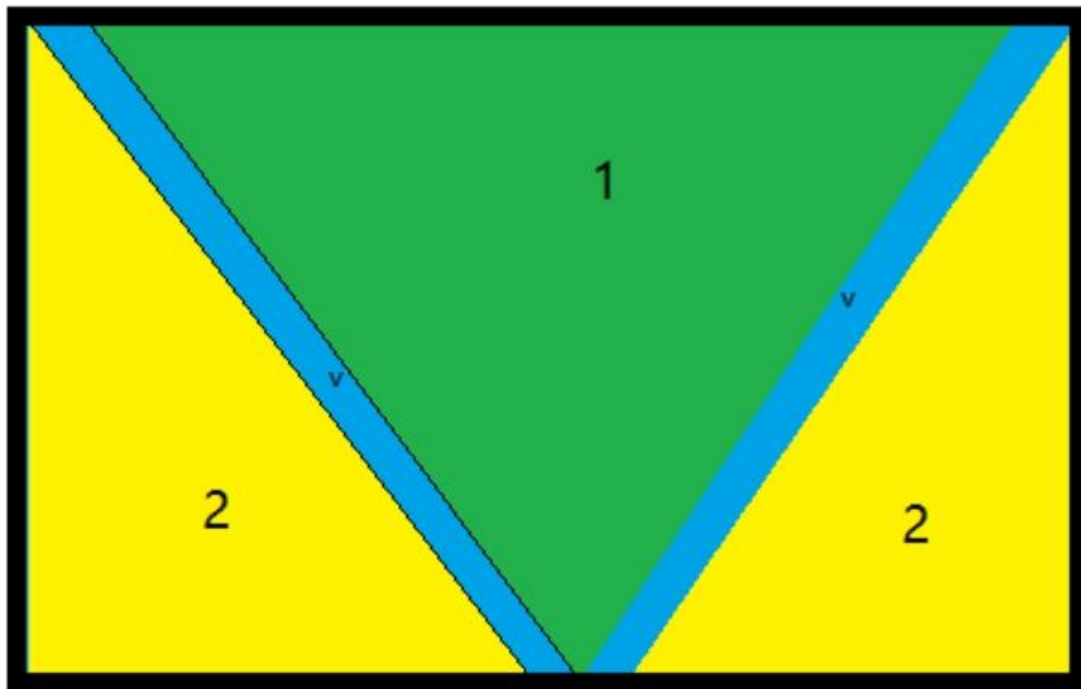The region of interest (ROI) covering the entire ventral part of the joint capsule was defined by the Polygon function within the software used. Within the ROI, the V-shaped and the adjacent reference area were identified and differentiated (Fig. 8).
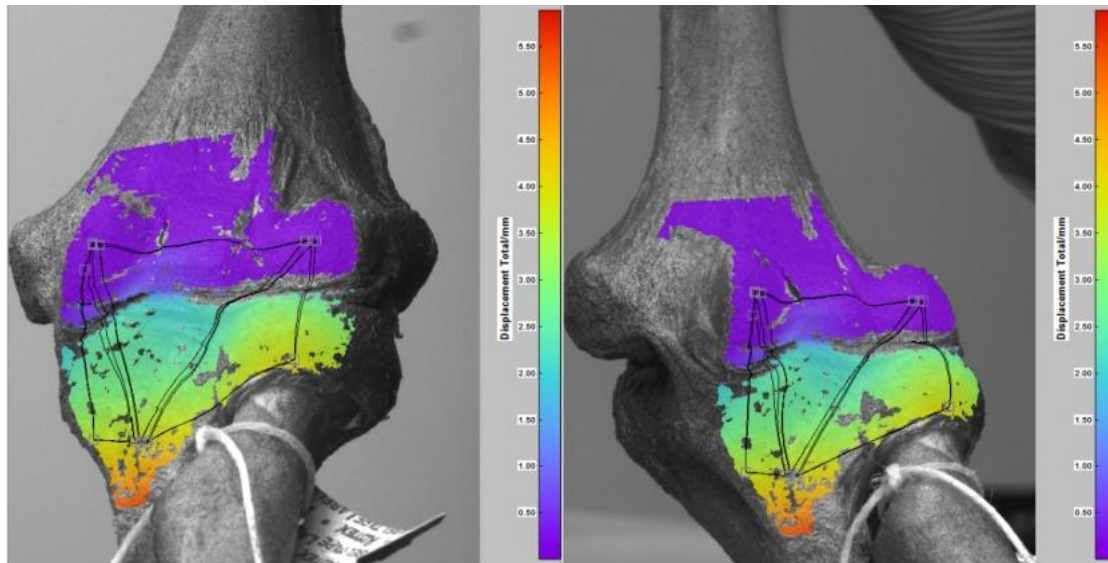
Fig. 8 ROI setting diagram

Delineation of V-shaped area：Specimen E02, -10°refers to 0°Total Displacement

The mean displacements of the point sets in the X-axis direction, Y-axis direction, and total displacement in these regions were derived.(1,2,V) By comparing the displacement data in all of these ROIs and by also performing statistical analysis, the stiffness differences between the V-shaped area and the surrounding tissues were compared. We hypothesized that the v-shape showed a different mean displacement in the direction of motion in which the capsule was stretched (Y-direction) when compared to the reference area. The direction of the X/Y- axis was set as shown in Fig. 9.
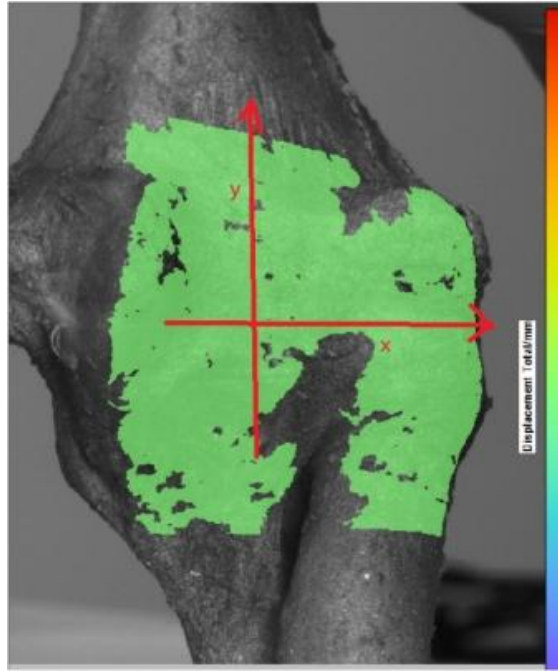
Fig. 9 X/Y- axis

The movement direction of the joint capsule being stretched is set to the y-axis direction, and the

direction perpendicular to it is the x-axis direction

2.1.3. Statistical Analysis

Descriptive statistics were used to aggregate and compare the data. Data were expressed as mean, median, or standard deviation (SD). Statistical analysis was performed using SPSS version 26.0 (IBM SPSS Statistics, USA). Non-parametric testing has no requirements for the overall distribution to be used in a broader range. After consideration of our sample size and test cases, a two-sample non-parametric test (Wilson Signed Rank Test) was applied to compare the differences between the displacement of the V-shaped ROI and the reference ROI. A p-value of less than 0.05 (2-sided significance testing) was considered statistically significant in all analyses.

Results

1. Results of Preliminary Image Analysis

1.1. Revisions

Due to the limitations of experimental conditions such as shadows, insufficient light, uneven speed, excessive deformation, and the error within the system algorithm, the evaluation conducted contained varying degrees of missing data. In the process of recording data from specimen E01 in the medial dorsal view, valid results were not obtained during subsequent evaluations even after making various adjustments due to some focusing problems and insufficient light. As the data was not sufficient for specimen E01 in the medial dorsal view, this view and sample were excluded.

There are still some blind spots in the results for the remaining specimens due to the various reasons mentioned previously. However, when combined with our unique inverse order approach, the results show coverage over the study area, therefore these were included in statistical calculations.

An example of the results from these experiments is illustrated. (Fig. 10-12)
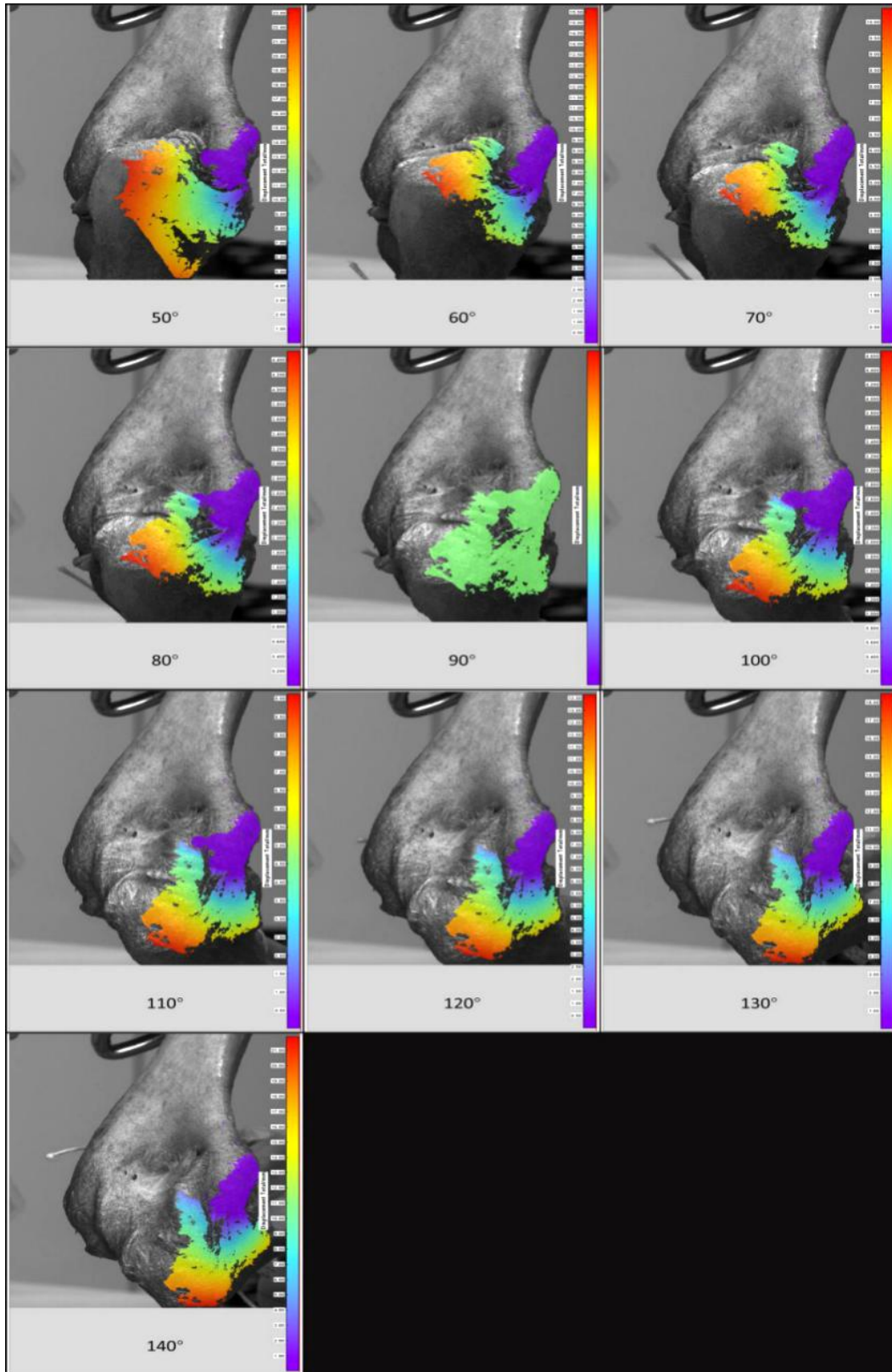
Fig. 10 Specimen E06, The medial dorsal view

Blue indicates less displacement, implying higher tissue tension and stability, while red shows

more displacement and laxity during movement
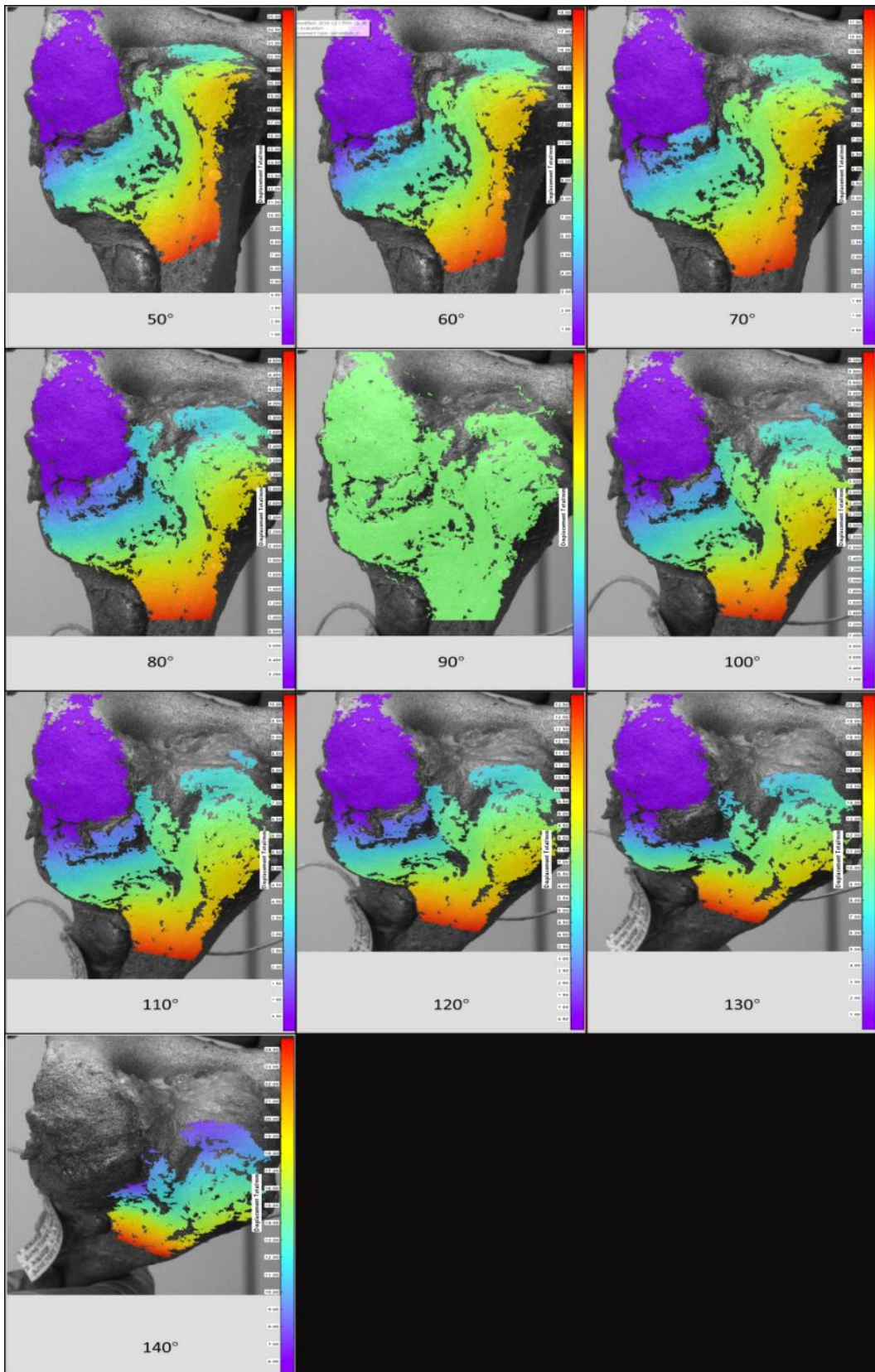
Fig. 11 Specimen E06, 90°refer to 50°Total Displacement, The lateral dorsal view

Blue indicates less displacement, implying higher tissue tension and stability, while red shows

more displacement and laxity during movement
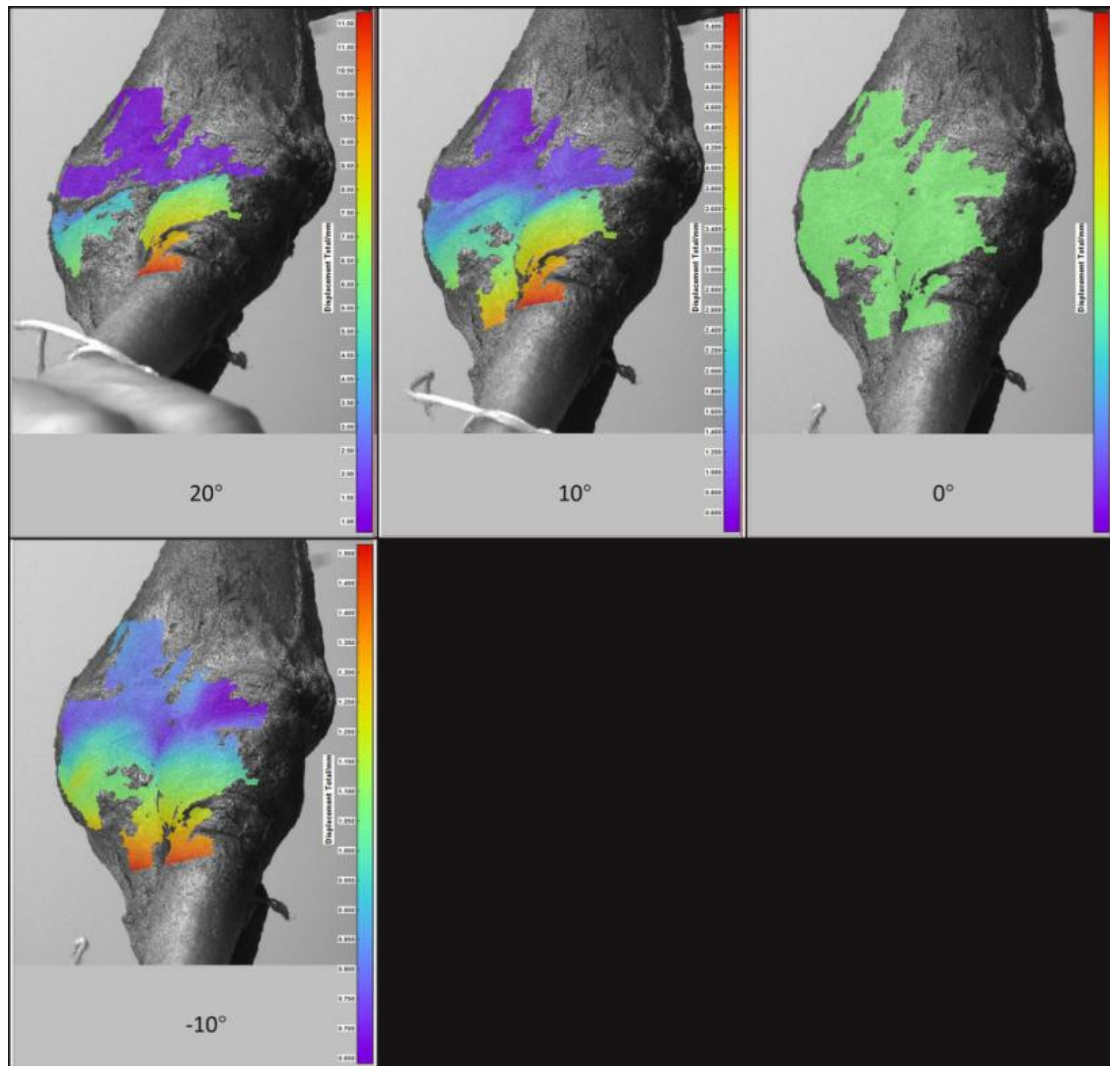
Fig. 12 Spicemen E06,　The ventral view

Blue indicates less displacement, implying higher tissue tension and stability, while red shows

more displacement and laxity during movement

1.2. General Description of Image Results

According to the total displacement graph, the changes in the elbow capsule during both flexion and extension can be clearly identified. The color blue represents less displacement, which suggests that this part of the tissue is more tense and stable. Contrary to this, the parts illustrated in red indicate more displacement and more laxity during movement.

In both dorsal views, the displacement of the surface increases gradually as the motion angle increases. The displacement changes on the surfaces of the joint capsules were uniformly distributed as a fan shape centered on the center of rotation. Closer to the center, less displacement was observed. No significant differences in tension were observed between them, except for the effect seen due to distance.

When the ventral view images were analysed, the rotation axis was orientated horizontally and a V-shaped region was present. The joint capsule tissue at the same distance from the rotation axis on the ventral side did not vary uniformly; there was a blue V-shaped structure in the middle part with the tip pointing towards the direction of the ulnar radius. As the elbow joints were moved in position from 30° of flexion through to 10° of hyperextension, the more extended V-shaped area became more pronounced. When the elbow joint was extended to its maximum, and the angle was no longer changing, the 'V' shape became increasingly faded as the force application continued.

2. Results of Depth Analysis

2.1. Revisions

For the same reasons mentioned previously, the data relating to 30° were not collected in their entirety. The sample size was too small to allow for a comparative test. For this reason, the data collected at 30° are only briefly described statistically and are not included in the hypothesis test.

2.2. Calculation of Displacement Values

Besides the total displacement, the data in both directions of the X-axis and Y-axis were calculated separately. The results are shown in Tab. 5-7 and Fig. 13-15.

Tab. 5 Average total displacement relative to the starting reference point (at 0°) at different angles for each ROI.

Flexion angle /(°)	ROI	Average displacement in the region/ mm						
		E01	E02	E03	E04	E05	E06	E07
30	1		-4.2615	-6.34917		-8.3164		-6.83062
	2	--	-8.434	-9.61954	--	-11.399	--	-8.06313
	1+2		-6.34775	-7.984355		-9.8577		-7.446875
	V		-5.3798	-7.50692		-9.8026		-7.557
20	1	-3.1051	-2.769	-4.31541	-2.71288	-6.2236	-4.19	-4.66095
	2	-7.29365	-5.4087	-6.3058	-6.9739	-8.3529	-6.3241	-5.50085
	1+2	-5.199375	-4.08885	-5.310605	-4.84339	-7.28825	-5.25705	-5.0809
	V	-4.92943	-3.4461	-5.0882	-4.6225	-7.3375	-5.2543	-5.1328
10	1	-1.72126	-1.3815	-2.70296	-1.16638	-3.5302	-2.2325	-2.4149
	2	-3.68694	-2.5385	-3.46523	-3.0145	-4.5355	-3.3389	-2.87898
	1+2	-2.7041	-1.96	-3.084095	-2.09044	-4.03285	-2.7857	-2.64694
	V	-2.56997	-1.7074	-3.03236	-2.0291	-4.0623	-2.7612	-2.6441
-10	1	2.66871	3.0409	2.87947	2.33877	1.0257	0.6017	2.719
	2	3.33291	4.1037	2.58078	3.4157	1.2056	1.1412	3.18403
	1+2	3.00081	3.5723	2.730125	2.877235	1.11565	0.87145	2.951515
	V	2.97015	3.6053	3.01307	2.8656	1.1965	0.9515	2.9766

Using 0 degrees as a reference, as the angle of movement increases from 0, the absolute displacement on the joint capsule surface also increases. Negative values indicated that the direction of displacement was opposite to the direction of motion.
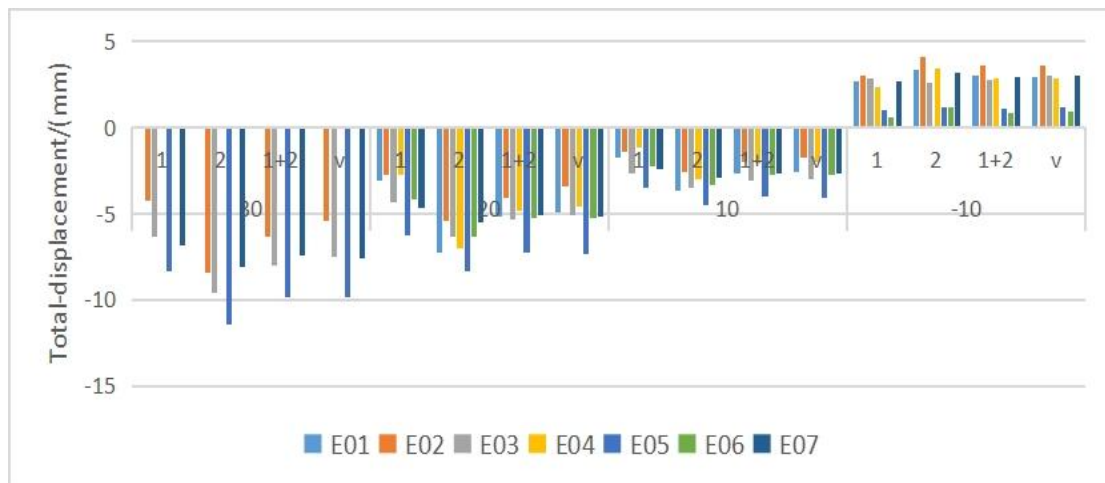

Fig. 13 Graphic of average total displacement relative to the starting reference point (at 0°) at different angles for each ROI.

Tab. 6 Average displacement in the y-axis direction relative to the starting reference point (at 0°) at different angles for each ROI.

Flexion angle /(°)	ROI	Average displacement in the region/ mm						
		E01	E02	E03	E04	E05	E06	E07
30	1	--	3.8448	4.30822	--	5.35845	--	3.86685
	2		7.607	6.2361		7.65824		3.70346
	1+2		5.7259	5.27216		6.508345		3.785155
	v		4.4268	4.72927		5.9482		3.94194
20	1	2.24168	2.664	2.48504	1.64107	3.83055	3.3358	2.16568
	2	4.06582	4.852	3.40488	4.41331	5.35162	5.1912	2.01204
	1+2	3.15375	3.758	2.94496	3.02719	4.591085	4.2635	2.08886
	v	3.04253	2.8894	1.91337	1.7986	4.2144	3.7965	2.15594
10	1	1.09244	1.2717	1.22465	0.56093	1.98825	1.6286	0.8958
	2	1.68016	2.1947	1.4885	1.53474	2.65223	2.5403	0.78589
	1+2	1.3863	1.7332	1.356575	1.047835	2.32024	2.08445	0.840845
	v	1.33436	1.3553	1.21208	0.4127	2.1113	1.8063	0.04844
-10	1	-1.5467	-2.34542	0.30965	-1.4647	-0.63178	0.1187	-1.44931
	2	-1.56744	-3.0913	0.31334	-1.75525	-0.88425	0.0088	-1.3187
	1+2	-1.55707	-2.71836	0.311495	-1.609975	-0.758015	0.06375	-1.384005
	v	-1.57063	-2.6548	0.32168	-1.3012	-0.6214	0.0911	-1.48854

Using 0 degrees as a reference, as the angle of movement increases from 0, the absolute displacement on the joint capsule surface also increases. Negative values indicated that the direction of displacement was opposite to the direction of motion.

Fig. 14 Graphic of average displacement in the y-axis direction relative to the starting reference point (at 0°) at different angles for each ROI.

Tab.7 Average displacement in the x-axis direction relative to the starting reference point (at 0°) at different angles for each ROI.

Flexion angle /(°)	ROI	Average displacement in the region/ mm						
		E01	E02	E03	E04	E05	E06	E07
30	1	--	-0.53415	-1.40054	--	-1.03174	--	-1.97466
	2		-0.39577	-1.58292		-1.36361		-1.85078
	1+2		-0.46496	-1.49173		-1.197675		-1.91272
	v		-0.417	-1.39955		-0.9773		-1.93603
20	1	-0.22838	-0.04242	-0.84999	-0.136	-0.45544	-0.8793	-1.65339
	2	-0.15424	0.113	-1.01196	-0.04341	-0.53547	-1.15666	-1.60262
	1+2	-0.19131	0.03529	-0.930975	-0.089705	-0.495455	-1.01798	-1.628005
	v	-0.20368	0.0024	-0.8918	-0.11444	-0.3582	-0.9468	-1.62903
10	1	-0.09576	-0.01782	-0.47299	-0.05126	-0.13924	-0.5836	-0.68663
	2	0.00129	0.08006	-0.53659	0.27659	-0.10336	-0.80606	-0.64789
	1+2	-0.047235	0.03112	-0.50479	0.112665	-0.1213	-0.69483	-0.66726
	v	-0.05106	-0.0112	-0.49309	0.05646	-0.0424	-0.663	-0.65163
-10	1	-0.51404	1.39343	6.42764	-0.083	-1.9409	-0.9962	-1.36884
	2	-0.61972	1.33809	6.50112	-0.18143	-1.93091	-0.97588	-1.51968
	1+2	-0.56688	1.36576	6.46438	-0.132215	-1.93591	-0.98604	-1.44426
	v	-0.5562	1.40429	6.44895	-0.08068	-2.0263	-1.039	-1.44797

Using 0 degrees as a reference, as the angle of movement increases from 0, the absolute displacement on the joint capsule surface also increases. Negative values indicated that the direction of displacement was opposite to the direction of motion.
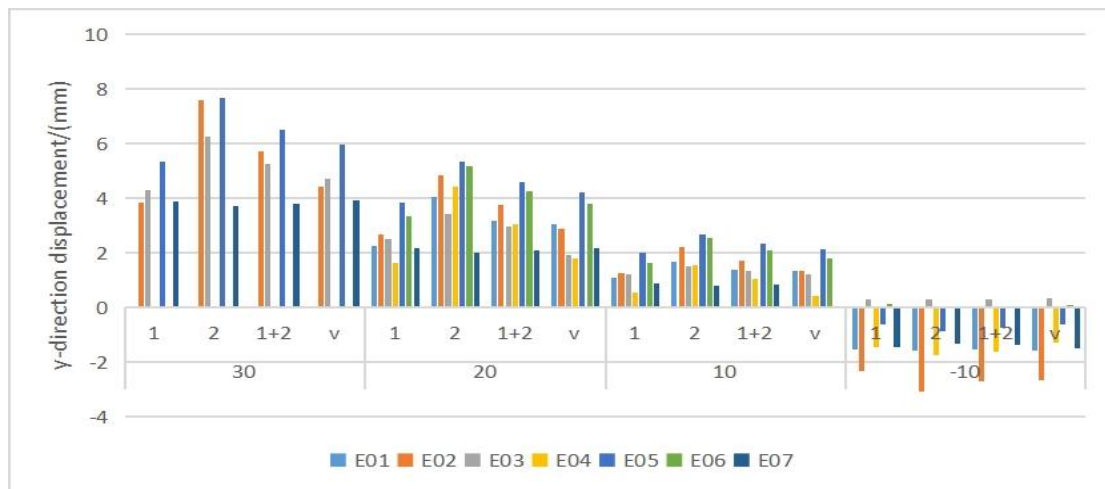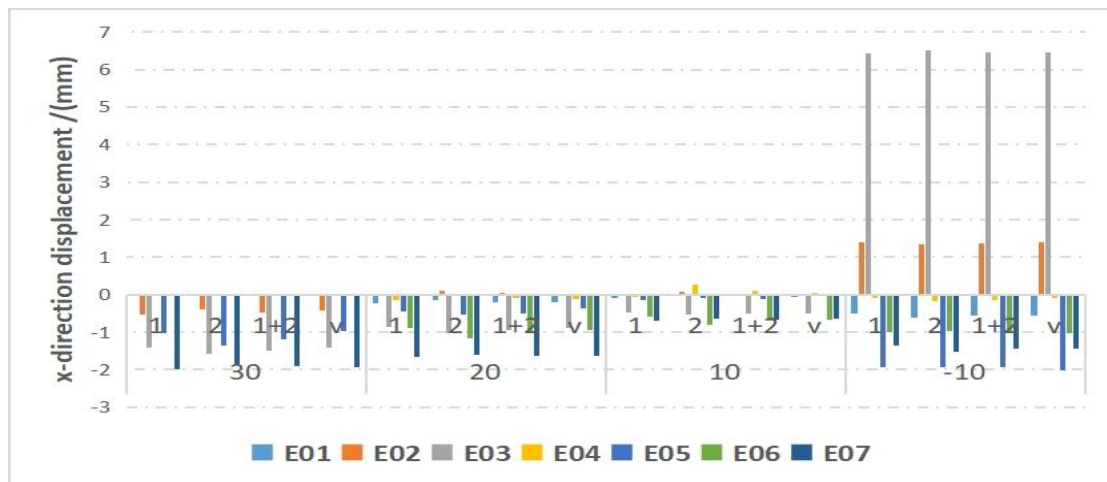

Fig. 15 Graphic of average displacement in the x-axis direction relative to the starting reference point (at 0°) at different angles for each ROI.

2.3. Statistical Analysis

A pairwise comparison between the average displacement of spots in the V-shaped ROI and adjacent ROI was performed by applying the non-parametric Wilcoxon signed-rank test. (Tab.8)

Negative values indicated that the direction of displacement was opposite to the direction of motion. When expressing the distance, only the absolute value was required. From Tab. 8, it can be observed that the mean and median were smaller than the reference area in the v-shape, with the exception of the total displacement at -10°, and in the X-axis displacement at 10°and -10°.

In the Y-axis dimension, when compared to 0°, the displacement of the v ROI at 10° and 20° was significantly lower than the displacement of the adjacent ROI. This phenomenon was not significant when the flexion angle was below 0°.

The X-axis displacement may be affected by movement from the device. The total displacement combines the X-axis data and the Y-axis data, so it also showed no difference.

The V zone acts as a stabilizer in elbow joint flexion and extension activities between 20° and 0°. But when the elbow joint was under hyperextension, there is no obvious evidence that it was essential

Tab.8 Statistical results data

Direction	Flexion angle /(°)	ROI	Mean	Median	SD	P-value(α=0.05)
Total displacement	30	V	-7.562	-7.532	1.806	--
		Adjacent	-7.909	-7.716	1.467	
	20	V	-5.116	-5.088	1.156	0.128
		Adjacent	-5.295	-5.199	0.974	
	10	V	-2.687	-2.644	0.755	0.063
		Adjacent	-2.758	-2.704	0.687	
	-10	V	2.511	2.970	1.013	0.091
		Adjacent	2.446	2.877	1.029	
Y-axis displacement	30	V	4.762	4.578	0.855	--
		Adjacent	5.323	5.499	1.145	
	20	V	2.830	2.889	0.936	**0.028**
		Adjacent	3.404	3.154	0.858	
	10	V	1.183	1.334	0.729	**0.018**
		Adjacent	1.538	1.386	0.537	
	-10	V	-1.032	-1.301	1.038	0.237
		Adjacent	-1.093	-1.384	1.051	
X-axis displacement	30	V	-1.182	-1.188	0.644	--
		Adjacent	-1.267	-1.345	0.610	
	20	V	-0.592	-0.358	0.589	0.499
		Adjacent	-0.617	-0.495	0.603	
	10	V	-0.270	-0.121	0.342	0.735
		Adjacent	-0.265	-0.051	0.322	
	-10	V	0.395	-0.567	2.878	0.612
		Adjacent	0.386	-0.556	2.890	

Mean and median were generally smaller in the V-shape, except for total displacement at

-10° and X-axis at 10°/-10°. In the Y-axis, V ROI displacement at 10°/20° was lower than

adjacent ROI at 0°. This wasn't significant below 0°. X-axis displacement may be due to device

movement. Total displacement (combining X and Y data) showed no difference.

Discussion

The stability of the elbow is crucial for maintaining its primary function. In the past, research on elbow joint stability has predominantly focused on the bony structures, ligaments, and muscles. The elbow capsule has been neglected and is therefore poorly understood. The elbow capsules contribution towards maintaining stability in the elbow joint has been confirmed by some scholars [3]. However, the exact mechanisms and focus of action have yet to be elucidated. The articular capsule consists of an internal synovial layer and an external fibrous membrane. The synovial layer is thin and soft, the inner surface is lined with synovial epithelium that secretes synovial fluid, and the fibrous layer consists of dense connective tissue. It is difficult to completely distinguish the joint capsule from the surrounding ligamentous tissue, and the ligaments that we have appointed and been familiar with in the past are concentrated on the medial and lateral sides of the elbow joint whilst the ventral and dorsal sides of the elbow joint have largely been ignored. Lee [32], tentatively predicted that the ventral and dorsal sides of the elbow capsule are not just a uniform patch of capsular fibrous connective tissue, therefore there are possibilities for further differentiation. This work identified six specific areas on the dorsal and ventral sides in relation to their fiber orientation as observed with the naked eye. These structures are most probably the key focus of the elbow capsule's function relating to joint stability. We aimed to provide an in-depth evaluation and validation of these areas, to investigate whether there are functional differences between the various parts of the elbow capsule during joint flexion and extension activities. In addition, new ligamentous structures can be identified with these techniques. The non-destructive, convenient, and precise advantages of the DIC method can further assist us in gaining a better understanding of these conditions, functions and structures.

1. Result Analysis

In the first phase of the experiment, the DIC method was used to obtain the total displacement during movement of the three surfaces of elbow capsule - the ventral,

dorsal medial, and dorsal lateral side. This represents an indirect representation of the stress on the surface. Less displacement denotes relatively more stability, and its role in maintaining stability during motion is greater. While we did not find significant differences in the results for the dorsal side, we found a visible and identifiable distinction between the stresses on the ventral side. This practical insight fits well with what we knew from the literature and had predicted about band delineation. In this regard, further experimental comparisons were also designed and outlined.

The results from the second phase of the experiment confirmed that the v-zone in the anterior joint capsule provided extra restrictive forces during elbow flexion and extension. This was seen mainly in the direction perpendicular to the axis of rotation, which is the stretching direction for the joint capsule. Although the bone structure can limit elbow hyperextension to a greater extent, it should also have a uniform surface change if the joint capsule does not provide additional force. This structure can therefore assist in limitation of elbow hyperextension. The structures corresponding to the v-zone are the anterior lateral band and the anterior medial oblique band.

2. Experimental Method Discussion

The images obtained in our first phase experiment did not suggest a distinction on the dorsal side of the joint capsule that is recognizable visually, but also this does not necessarily confirm the absence of a specific anatomical region in the dorsal region of the elbow capsule.

Currently the DIC method is mainly applied during analysis of small deformation and small displacement. In contrast, the joint capsule deformation undertaken during this experiment would be classified as a big deformation. Wide angular rotation of the joint also occurs during big displacement in the stereoscopic dimension. In particular, the study of the dorsal joint capsule has a range of motion up to 90, and the shape of the dorsal elbow capsule also approximates a trigonal cone which is not in one plane only. This limitation was not fully considered during the experimental design stages; therefore, in some images, it was not possible to find the

unique sharp correlation peak during the process of matching using the correlation function in order to search for the matching points. To solve the impact of this big deformation problem on the correlation calculation, the main idea revolved around decomposing the bigger deformation of the overall phase into minor deformations enabling calculation by updating the reference map. Nevertheless, the calculation results from the correlation of the new reference map may itself carry the errors caused by interpolation. Moreover, every time the reference map changes, a certain number of errors would be expected and introduced, thus causing an accumulation of errors. The direct consequence is that after several reference map transformations, the position of the selected points and the final calculated points may have large deviations, resulting in uncertainty drift of the relevant calculation results. Therefore, research into the related algorithm has yet to be improved in depth and requires work.

Moreover, if conditions permit, a multi-camera system should be considered in order to achieve larger orientation angles, 360° panoramic measurements could even be utilized to solve the problem in stereoscopic space such as for large angle rotation of joints.

There may also be limitations in the measurement conditions. These may include noise from the camera sensor, lack of clarity of the spot, poor lighting, uneven movement speed or lack of stability of the device, etc., which may lead to reduced correlations. As a result, the traceable patterns could be absent, or the corresponding settings may not be present thus preventing the initial stages of evaluation.

In contrast, the study of the anterior joint capsule was relatively more circumscribed to one plane in terms of movement angle and shape. Correlations were satisfactory over the entire measurement, even when bigger displacements and deformations were related. The correlation surface covered the ROI, and correlation loss was less than 5.7% of the initial associated surface. Although DIC suffers from some frequent uncorrelated gaps, there are still great advantages in evaluating the full field compared to other measurement techniques (e.g., strain gauges) that measure the strain alone at selected points whilst ignoring the rest of the surface.

3. Research Deficiencies and Improvements

Our specimens were not fresh frozen specimens, therefore the distinctions between the fiber orientations on the dorsal side were no longer apparent, which means it was not possible to identify the individual bands with the naked eye. Furthermore, its mechanical properties also differed from those of real human tissue. This study used a relatively large number of specimens, and many different variables such as angles and different views were explored. These were implemented mainly to screen the subjects and to clarify the direction of the study. Studies concerning the ventral joint capsule or other sides of the elbow could be further developed on fresh frozen specimens. A comparison of different treatments could also be used to quantify the percentage contribution of v-bands towards elbow joint stability. This finding can also be made more convincing by combining it with relevant histological validation.

4. Clinical Applications

In clinical practice, we should pay attention to protecting and strengthening this part of the joint capsule during surgical treatment. Although the anterior approach to the elbow joint is not frequently used in open surgery because of the complex neurovascular distribution of the anterior capsule, there is no substitute for exposing the vascular and neurological structures of the elbow fossa as well as exposing the bony structures located anteromedially. Examples include anterior approach exploration of the brachial artery and median nerve and treating fractures of the ulnar coronoid process and radial head. In such surgeries that necessitate an anterolateral approach, we can try to avoid disruption of this area, especially if other underlying mechanisms of elbow instability are already present. Even if the disruption cannot be prevented, we should not abandon the repair of these areas.

Elbow arthroscopy is even more complicated. The elbow joint cavity gap is irregular, narrow, and curved, etc. The surrounding structures are dense, and important blood vessels and nerves are interspersed, so many factors are considered. Fortunately, the arthroscopic approach causes less injury to the soft tissues and relatively less

damage to the mechanical structures. However, conversely the repair we can do after destroying the joint capsule is also limited.

Also, when treating patients with elbow stiffness who undergo elbow release, the question of whether or not to remove the entire joint capsule, where to cut the capsule from, etc., needs to be reexamined.

When planning a postoperative rehabilitation program, what is the right time to start activity training? What direction and what degree of activity training? These also need to consider the effects of non-optimal joint capsule status.

Overall we need to take into account the influence of the anterolateral joint capsule of the elbow joint on its stability in a comprehensive manner to select the most appropriate clinical decision.

Conclusion

1. There are differences in the mechanical effects of the ventral joint capsule during elbow flexion and extension, and its contribution to elbow joint stability can be further investigated.

2. Two bands within the ventral joint capsule comprising the V-zone could provide more stability in the vertical direction. We can perform further experimental verification accordingly with a view to demonstrating whether these two bands can be named as ligaments.

3. No significant difference was found in the contribution of the dorsal joint capsule to the stability of the elbow joint during flexion and extension.

Summary

Introduction

The stability of the elbow joint is maintained by the bones, joints, ligaments, and joint capsule that make up the articulation. As the joint between the shoulder and the wrist, maintaining stability in the elbow joint is important for the accomplishment of upper extremity functions. The role of bones, joints, and ligaments on the stability of the elbow joint is self-evident, but the influence of the joint capsule on the stability of the elbow joint is less well understood. In this thesis, based on the morphological and structural characteristics of the elbow joint capsule in applied anatomy, the role of the various parts of the elbow joint capsule in maintaining the stability of the elbow joint is studied from a biomechanical perspective. the aim is to provide an anatomical basis for the clinical understanding and treatment of acute and chronic elbow instability.

Methods

Seven intact elbow cadavers with only capsular ligamentous coverings (no evidence of previous surgery or injury to these specimens) were recorded and biomechanically tested as follows. The changes in the surface of the elbow capsule during motion were recorded for each perspective in a specific angular range using a DIC device: -10 to 30° in the ventral part, 50 to 140° in the medial and lateral part. After we obtained all the displacement field maps, we found that the presence of special v shape is consistent with the hypothesis of previous scholars on the structure of the ventral joint capsule. We accordingly do a comparison of the displacement of the special v structure with that of the surrounding tissue in different axial dimensions. The resulting data were statistically analyzed using Wilson Signed Rank Test.

Results and Conclusion

No significant difference was found in the contribution of the dorsal joint capsule to the stability of the elbow joint during flexion and extension. There were differences in

the mechanical effects of various components of the ventral joint capsule during elbow flexion and extension, and we further investigated the contribution of a specific V-zone to elbow joint stability. Two bands within the ventral joint capsule comprising the V-zone could provide more stability in the vertical direction. We can perform further experimental verification in fresh frozen cadaveric specimen to demonstrate whether these two bands can be named as ligaments.

Zusammenfassung

Einleitung

Die Stabilität des Ellenbogengelenks wird durch die Knochen, Gelenke, Bänder und die Gelenkkapsel gewährleistet, aus denen das Gelenk besteht. Als Gelenk zwischen Schulter und Handgelenk ist die Aufrechterhaltung der Stabilität des Ellenbogengelenks wichtig für die Ausführung der Funktionen der oberen Extremität. Die Rolle der Knochen, Gelenke und Bänder für die Stabilität des Ellenbogengelenks ist offensichtlich, aber der Einfluss der Gelenkkapsel auf die Stabilität des Ellenbogengelenks ist weniger gut bekannt. In dieser Arbeit wird, ausgehend von den morphologischen und strukturellen Merkmalen der Ellenbogengelenkkapsel in der angewandten Anatomie, die Rolle der verschiedenen Teile der Ellenbogengelenkkapsel bei der Aufrechterhaltung der Stabilität des Ellenbogengelenks aus biomechanischer Sicht untersucht. , Ziel ist es, eine anatomische Grundlage für das klinische Verständnis und die Behandlung der akuten und chronischen Ellenbogeninstabilität zu schaffen.

Methoden

Sieben Ellenbogenkadaver mit ausschließlich der kapsuloligamentären Hülle (bei keinem der Probanden gab es Hinweise auf eine frühere Operation oder Verletzung des Ellenbogens) wurden wie folgt aufgenommen und biomechanisch getestet. Die Veränderungen der Oberfläche der Ellenbogenkapsel während der Bewegung wurden für jede Perspektive in einem bestimmten Winkelbereich mit einem DIC-Gerät aufgezeichnet: -10 bis 30° im ventralen Teil, 50 bis 140° im medialen und lateralen Teil. Nachdem wir alle Verschiebungsfelder erhalten hatten, stellten wir fest, dass eine markante v-förmige Ungleichmäßigkeit in den Verschiebungsfeldern mit der Hypothese früherer Wissenschaftler über die Struktur der ventralen Gelenkkapsel übereinstimmt. Dementsprechend haben wir die Verschiebung der speziellen V-Struktur mit der des umgebenden Gewebes in verschiedenen axialen Dimensionen

verglichen. Die daraus resultierenden Daten wurden mit dem Wilson Signed Rank Test statistisch ausgewertet.

Ergebnisse und Schlussfolgerung

Es wurde kein signifikanter Unterschied im Beitrag der dorsalen Gelenkkapsel zur Stabilität des Ellenbogengelenks bei Beugung und Streckung festgestellt. Es gab Unterschiede in den mechanischen Effekten verschiedener Komponenten der ventralen Gelenkkapsel während der Beugung und Streckung des Ellenbogens, und wir untersuchten weiter den Beitrag einer bestimmten V-Zone zur Stabilität des Ellenbogengelenks. Zwei Stränge innerhalb der ventralen Gelenkkapsel, die die V-Zone bilden, könnten für mehr Stabilität in vertikaler Richtung sorgen. Wir können weitere Experimente mit frisch gefrorenen Leichenpräparaten durchführen, um zu testen, ob diese beiden Stränge als Bänder bezeichnet werden können.

Reference

[1]   Q. Liu, "Reconstruction of elbow flexion and elbow functional evaluation,"
        Orthop. J. China, vol. 05, pp. 501–502, 2002.

[2]   A. Assiotis, A. M. Khan, A. R. Sankey, and R. Dattani, "Elbow dislocations,"
        Br. J. Hosp. Med., vol. 80, no. 7, pp. C98–C102, Jul. 2019, doi:
        10.12968/hmed.2019.80.7.C98.

[3]   M. R. Safran and D. Baillargeon, "Soft-tissue stabilizers of the elbow," in
        Journal of Shoulder and Elbow Surgery, 2005, vol. 14, no. 1 SUPPL., pp.
        S179–S185, doi: 10.1016/j.jse.2004.09.032.

[4]   S. Tyrdal and B. S. Olsen, "Hyperextension of the elbow joint: Pathoanatomy
        and kinematics of ligament injuries," *J. Shoulder Elb. Surg.*, vol. 7, no. 3, pp.
        272–283, 1998, doi: 10.1016/S1058-2746(98)90056-8.

[5]   A. L. Aquilina and A. J. Grazette, "Clinical Anatomy and Assessment of the
        Elbow," *Open Orthop. J.*, vol. 11, no. 1, pp. 1347–1352, 2017, doi:
        10.2174/1874325001711011347.

[6]   R. A. Kaufmann, T. Wilps, V. Musahl, and R. E. Debski, "Elbow
        Biomechanics: Soft Tissue Stabilizers," *Journal of Hand Surgery*, vol. 45, no. 2.
        pp. 140–147, 2020, doi: 10.1016/j.jhsa.2019.10.034.

[7]   M. J. O'Brien and F. H. Savoie, "Arthroscopic and open management of
        posterolateral rotatory instability of the elbow," *Sports Medicine and
        Arthroscopy Review*, vol. 22, no. 3. Sports Med Arthrosc Rev, pp. 194–200,
        2014, doi: 10.1097/JSA.0000000000000029.

[8]   C. L. Camp, J. Sanchez-Sotelo, M. N. Shields, and S. W. O'Driscoll, "Lateral
        Ulnar Collateral Ligament Reconstruction for Posterolateral Rotatory
        Instability of the Elbow," *Arthrosc. Tech.*, vol. 6, no. 4, pp. e1101–e1105, 2017,
        doi: 10.1016/j.eats.2017.03.029.

[9]   C. Schaeffeler, S. Waldt, and K. Woertler, "Traumatic instability of the elbow -

Anatomy, pathomechanisms and presentation on imaging," *Eur. Radiol.*, vol. 23, no. 9, pp. 2582–2593, 2013, doi: 10.1007/s00330-013-2855-5.

[10] K. Kimata, M. Yasui, H. Yokota, S. Hirai, M. Naito, and T. Nakano, "Transverse ligament of the elbow joint: an anatomic study of cadavers," *J. Shoulder Elb. Surg.*, vol. 28, no. 11, pp. 2253–2258, 2019, doi: 10.1016/j.jse.2019.04.048.

[11] S. Floris, B. S. Olsen, M. Dalstra, J. O. Søjbjerg, and O. Sneppen, "The medial collateral ligament of the elbow joint: Anatomy and kinematics," *J. Shoulder Elb. Surg.*, vol. 7, no. 4, pp. 345–351, 1998, doi: 10.1016/S1058-2746(98)90021-0.

[12] S. J. Frangiamore, K. Bigart, T. Nagle, R. Colbrunn, A. Millis, and M. S. Schickendantz, "Biomechanical analysis of elbow medial ulnar collateral ligament tear location and its effect on rotational stability," *J. Shoulder Elb. Surg.*, vol. 27, no. 11, pp. 2068–2076, 2018, doi: 10.1016/j.jse.2018.05.020.

[13] A. Prasad, D. D. Robertson, G. B. Sharma, and D. A. Stone, "Elbow: The trochleogingylomoid joint," *Seminars in Musculoskeletal Radiology*, vol. 7, no. 1. Semin Musculoskelet Radiol, pp. 19–25, 2003, doi: 10.1055/s-2003-41082.

[14] M. Sardelli, R. Z. Tashjian, and B. A. MacWilliams, "Functional elbow range of motion for contemporary tasks," *J. Bone Jt. Surg. - Ser. A*, vol. 93, no. 5, pp. 471–477, Mar. 2011, doi: 10.2106/JBJS.I.01633.

[15] R. K. Beals, "The Normal Carrying Angle of the Elbow A Radiographic Study of 422 Patients," *Clin. Orthop. Relat. Res.*, vol. 119, pp. 194–196, 1976, [Online]. Available: https://journals.lww.com/clinorthop/Fulltext/1976/09000/The_Normal_Carryin g_Angle_of_the_Elbow_A.28.aspx.

[16] W. Regan and B. Morrey, "Fractures of the coronoid process of the ulna," *J. Bone Jt. Surg. - Ser. A*, vol. 71, no. 9, pp. 1348–1354, Oct. 1989, doi: 10.2106/00004623-198971090-00011.

[17] J. L. Matzon, B. J. Widmer, L. F. Draganich, D. P. Mass, and C. S. Phillips, "Anatomy of the Coronoid Process," *J. Hand Surg. Am.*, vol. 31, no. 8, pp.

1272–1278, 2006, doi: 10.1016/j.jhsa.2006.05.010.

[18]   D. Ring, "Fractures of the Coronoid Process of the Ulna," *Journal of Hand Surgery*, vol. 31, no. 10. pp. 1679–1689, 2006, doi: 10.1016/j.jhsa.2006.08.020.

[19]   D. M. Beingessner, C. E. Dunning, R. A. Stacpoole, J. A. Johnson, and G. J. W. King, "The effect of coronoid fractures on elbow kinematics and stability," *Clin. Biomech.*, vol. 22, no. 2, pp. 183–190, 2007, doi: 10.1016/j.clinbiomech.2006.09.007.

[20]   S. W. O'Driscoll, J. B. Jupiter, M. S. Cohen, D. Ring, and M. D. McKee, "Difficult elbow fractures: pearls and pitfalls.," *Instr. Course Lect.*, vol. 52, pp. 113–134, 2003.

[21]   J. W. Pollock, J. Brownhill, L. Ferreira, C. P. McDonald, J. Johnson, and G. King, "The effect of anteromedial facet fractures of the coronoid and lateral collateral ligament injury on elbow stability and kinematics," *J. Bone Jt. Surg. - Ser. A*, vol. 91, no. 6, pp. 1448–1458, Jun. 2009, doi: 10.2106/JBJS.H.00222.

[22]   T. H. Bell, L. M. Ferreira, C. P. McDonald, J. A. Johnson, and G. J. W. King, "Contribution of the olecranon to elbow stability: An in vitro biomechanical study," *J. Bone Jt. Surg. - Ser. A*, vol. 92, no. 4, pp. 949–957, Apr. 2010, doi: 10.2106/JBJS.H.01873.

[23]   K. Wegmann *et al.*, "The shape match of the olecranon tip for reconstruction of the coronoid process: influence of side and osteotomy angle," *J. Shoulder Elb. Surg.*, vol. 28, no. 4, pp. e117–e124, 2019, doi: 10.1016/j.jse.2018.10.022.

[24]   B. Alolabi, A. Gray, L. M. Ferreira, J. A. Johnson, G. S. Athwal, and G. J. W. King, "Reconstruction of the coronoid process using the tip of the ipsilateral olecranon," *J. Bone Jt. Surg. - Ser. A*, vol. 96, no. 7, pp. 590–596, Apr. 2014, doi: 10.2106/JBJS.L.00698.

[25]   B. F. Morrey and K. N. An, "Articular and ligamentous contributions to the stability of the elbow joint," *Am. J. Sports Med.*, vol. 11, no. 5, pp. 315–319, 1983, doi: 10.1177/036354658301100506.

[26]   J. A. Hall and M. D. McKee, "Posterolateral rotatory instability of the elbow following radial head resection," *J. Bone Jt. Surg. - Ser. A*, vol. 87, no. 7, pp.

1571–1579, Jul. 2005, doi: 10.2106/JBJS.D.02829.

[27]   A. G. Schneeberger, M. M. Sadowski, and H. A. C. Jacob, "Coronoid Process and Radial Head as Posterolateral Rotatory Stabilizers of the Elbow," *J. Bone Jt. Surg. - Ser. A*, vol. 86, no. 5, pp. 975–982, 2004, doi: 10.2106/00004623-200405000-00013.

[28]   M. F. Shepard, K. L. Markolf, and A. Mallik Dunbar, "Effects of radial head excision and distal radial shortening on load-sharing in cadaver forearms," *J. Bone Jt. Surg. - Ser. A*, vol. 83, no. 1, pp. 92–100, 2001, doi: 10.2106/00004623-200101000-00013.

[29]   B. F. Morrey, "Complex instability of the elbow.," *Instructional course lectures*, vol. 47. Instr Course Lect, pp. 157–164, 1998, doi: 10.1016/b978-1-4160-2902-1.50034-6.

[30]   A. Badre, D. T. Axford, S. Banayan, J. A. Johnson, and G. J. W. King, "Role of the anconeus in the stability of a lateral ligament and common extensor origin–deficient elbow: an in vitro biomechanical study," *J. Shoulder Elb. Surg.*, vol. 28, no. 5, pp. 974–981, 2019, doi: 10.1016/j.jse.2018.11.040.

[31]   F. Lin, N. Kohli, S. Perlmutter, D. Lim, G. W. Nuber, and M. Makhsous, "Muscle contribution to elbow joint valgus stability," *J. Shoulder Elb. Surg.*, vol. 16, no. 6, pp. 795–802, 2007, doi: 10.1016/j.jse.2007.03.024.

[32]   L. M. Reichel and O. A. Morales, "Gross anatomy of the elbow capsule: A cadaveric study," *J. Hand Surg. Am.*, vol. 38, no. 1, pp. 110–116, 2013, doi: 10.1016/j.jhsa.2012.09.031.

[33]   G. J. W. King, B. F. Morrey, and K. N. An, "Stabilizers of the elbow," *Journal of Shoulder and Elbow Surgery*, vol. 2, no. 3. Mosby, pp. 165–174, May 01, 1993, doi: 10.1016/S1058-2746(09)80053-0.

[34]   C. Dos Remedios, C. Chantelot, H. Migaud, D. Le Nen, C. Fontaine, and B. Landjerit, "Effect of anterior and posterior capsule release on elbow joint stability: An experimental study," *Rev. Chir. Orthop. Reparatrice Appar. Mot.*, vol. 89, no. 8, pp. 693–698, 2003, Accessed: Aug. 15, 2021. [Online]. Available:

https://pubmed-ncbi-nlm-nih-gov.proxy.library.carleton.ca/14726835/.

[35] H. Liu and P. Tang, "Instability of the elbow joint," *Int. J. Orthop.*, vol. 036, no. 005, pp. 340–343, 2015.

[36] K. K. Nielsen and B. S. Olsen, "No stabilizing effect of the elbow joint capsule. A kinematic study," *Acta Orthop. Scand.*, vol. 70, no. 1, pp. 6–8, 1999, doi: 10.3109/17453679909000947.

[37] B. S. Olsen, M. T. Vaesel, J. O. Søjbjerg, P. Helmig, and O. Sneppen, "Lateral collateral ligament of the elbow joint: anatomy and kinematics.," *J. Shoulder Elbow Surg.*, vol. 5, no. 2 Pt 1, pp. 103–112, Mar. 1996, doi: 10.1016/s1058-2746(96)80004-8.

[38] H. Shimura *et al.*, "Joint capsule attachment to the coronoid process of the ulna: an anatomic study with implications regarding the type 1 fractures of the coronoid process of the O'Driscoll classification," *J. Shoulder Elb. Surg.*, 2016, doi: 10.1016/j.jse.2016.01.024.

[39] D. S. Edwards, M. S. Arshad, T. Luokkala, A. E. Kedgley, and A. C. Watts, "The contribution of the posterolateral capsule to elbow joint stability: a cadaveric biomechanical investigation," *J. Shoulder Elb. Surg.*, 2018, doi: 10.1016/j.jse.2018.02.045.

[40] S. W. O'Driscoll, "Classification and evaluation of recurrent instability of the elbow," in *Clinical Orthopaedics and Related Research*, 2000, vol. 370, no. 370, pp. 34–43, doi: 10.1097/00003086-200001000-00005.

[41] P. O. Josefsson and B. E. Nilsson, "Incidence of elbow dislocation," *Acta Orthop.*, vol. 57, no. 6, pp. 537–538, 1986, doi: 10.3109/17453678609014788.

[42] M. DiPaola, W. B. Geissler, and A. L. Osterman, "Complex Elbow Instability," *Hand Clinics*, vol. 24, no. 1. Hand Clin, pp. 39–52, Feb. 2008, doi: 10.1016/j.hcl.2007.11.010.

[43] P. Tarassoli, P. McCann, and R. Amirfeyz, "Complex instability of the elbow," *Injury*, vol. 48, no. 3. Injury, pp. 568–577, Mar. 01, 2017, doi: 10.1016/j.injury.2013.09.032.

[44] Z. Hamoodi, J. Singh, M. H. Elvey, and A. C. Watts, "Reliability and validity

of the Wrightington classification of elbow fracture-dislocation," *Bone Jt. J.*, vol. 102, no. 8, pp. 1041–1047, Aug. 2020, doi: 10.1302/0301-620X.102B8.BJJ-2020-0013.R1.

[45] Z. Hamoodi, J. Singh, M. Elvey, and A. C. Watts, "Functional Outcomes of Elbow Injuries Managed According to the Wrightington Classification of Elbow Fracture Dislocations," *JSES Open Access*, vol. 3, no. 4, pp. 252–253, Dec. 2019, doi: 10.1016/j.jses.2019.10.075.

[46] M. A. Kuhn and G. Ross, "Acute elbow dislocations.," *Orthop. Clin. North Am.*, vol. 39, no. 2, pp. 155–61, v, Apr. 2008, doi: 10.1016/j.ocl.2007.12.004.

[47] J. W. Stoneback, B. D. Owens, J. Sykes, G. S. Athwal, L. Pointer, and J. M. Wolf, "Incidence of elbow dislocations in the United States population," *J. Bone Jt. Surg. - Ser. A*, vol. 94, no. 3, pp. 240–245, 2012, doi: 10.2106/JBJS.J.01663.

[48] J. E. Conway, F. W. Jobe, R. E. Glousman, and M. Pink, "Medial instability of the elbow in throwing athletes. Treatment by repair or reconstruction of the ulnar collateral ligament.," *JBJS*, vol. 74, no. 1, 1992, [Online]. Available: https://journals.lww.com/jbjsjournal/Fulltext/1992/74010/Medial_instability_of _the_elbow_in_throwing.9.aspx.

[49] T. L. Mehlhoff, P. C. Noble, J. B. Bennett, and H. S. Tullos, "Simple dislocation of the elbow in the adult. Results after closed treatment.," *JBJS*, vol. 70, no. 2, 1988, [Online]. Available: https://journals.lww.com/jbjsjournal/Fulltext/1988/70020/Simple_dislocation_ of_the_elbow_in_the_adult_.13.aspx.

[50] D. M. Kalainov and M. S. Cohen, "Posterolateral rotatory instability of the elbow in association with lateral epicondylitis: A report of three cases," *J. Bone Jt. Surg. - Ser. A*, vol. 87, no. 5, pp. 1120–1125, May 2005, doi: 10.2106/JBJS.D.02293.

[51] C. L. Camp, S. W. O'Driscoll, M. K. Wempe, and J. Smith, "The Sonographic Posterolateral Rotatory Stress Test for Elbow Instability: A Cadaveric Validation Study," *PM R*, vol. 9, no. 3, pp. 275–282, Mar. 2017, doi:

10.1016/j.pmrj.2016.06.014.

[52]   S. W. O'Driscoll, D. F. Bell, and B. F. Morrey, "Posterolateral rotatory
        instability of the elbow.," *JBJS*, vol. 73, no. 3, 1991, [Online]. Available:
        https://journals.lww.com/jbjsjournal/Fulltext/1991/73030/Posterolateral_rotator
        y_instability_of_the_elbow_.15.aspx.

[53]   E. Bellato *et al.*, "Role of the lateral collateral ligament in posteromedial
        rotatory instability of the elbow," *J. Shoulder Elb. Surg.*, vol. 26, no. 9, pp.
        1636–1643, 2017, doi: 10.1016/j.jse.2017.04.011.

[54]   M. H. Ebrahimzadeh, H. Amadzadeh-Chabock, and D. Ring, "Traumatic
        Elbow Instability," *J. Hand Surg. Am.*, vol. 35, no. 7, pp. 1220–1225, 2010, doi:
        10.1016/j.jhsa.2010.05.002.

[55]   L. E. Karbach and J. Elfar, "Elbow Instability: Anatomy, Biomechanics,
        Diagnostic Maneuvers, and Testing," *Journal of Hand Surgery*, vol. 42, no. 2.
        pp. 118–126, 2017, doi: 10.1016/j.jhsa.2016.11.025.

[56]   D. R. Shukla, E. Golan, M. C. Weiser, P. Nasser, J. Choueka, and M. Hausman,
        "The Posterior Bundle's Effect on Posteromedial Elbow Instability After a
        Transverse Coronoid Fracture: A Biomechanical Study," *J. Hand Surg. Am.*,
        vol. 43, no. 4, pp. 381.e1-381.e8, 2018, doi: 10.1016/j.jhsa.2017.09.018.

[57]   B. F. Morrey, "Reconstruction of the posterior bundle of the medial collateral
        ligament: A solution for posteromedial olecranon deficiency-a case report," *J.
        Shoulder Elb. Surg.*, vol. 21, no. 11, pp. e16–e19, 2012, doi:
        10.1016/j.jse.2012.08.021.

[58]   E. J. Golan, D. R. Shukla, P. Nasser, and M. Hausman, "Isolated ligamentous
        injury can cause posteromedial elbow instability: a cadaveric study," *J.
        Shoulder Elb. Surg.*, vol. 25, no. 12, pp. 2019–2024, 2016, doi:
        10.1016/j.jse.2016.04.022.

[59]   M. J. Gluck, C. M. Beck, E. J. Golan, P. Nasser, D. R. Shukla, and M. R.
        Hausman, "Varus posteromedial rotatory instability: a biomechanical analysis
        of posterior bundle of the medial ulnar collateral ligament reconstruction," *J.
        Shoulder Elb. Surg.*, vol. 27, no. 7, pp. 1317–1325, 2018, doi:

10.1016/j.jse.2018.02.058.

[60] M. E. Torchia and N. M. DiGiovine, "Anterior dislocation of the elbow in an arm wrestler," *J. Shoulder Elb. Surg.*, vol. 7, no. 5, pp. 539–541, 1998, doi: 10.1016/S1058-2746(98)90209-9.

[61] B. D. Martin, J. A. Johansen, and S. G. Edwards, "Complications Related to Simple Dislocations of the Elbow," *Hand Clinics*, vol. 24, no. 1. pp. 9–25, 2008, doi: 10.1016/j.hcl.2007.11.013.

[62] X. Liu, Y. Wei, and Z. Wang, "Biomechanics of orthopaedics and traumatology.," 2010.

[63] Z. Chen and S. Wu, "Plain analysis of strain measurement method with bonding resistance.," *Meas. Technol.*, vol. 8, pp. 24–26, 2002.

[64] Z. Jiang and Y. Fan, "Biomechanics-from basic to frontiers.," 2010.

[65] W. Xie, J. Zhou, and Q. Wang, "Development and application of Photoelastic method.," *Mod. Phys.*, vol. 3, pp. 34–36, 2006.

[66] Z. Lei, D. Yun, and Y. Kang, "Areview of digital photoelasticity.," *J. Exp. Mech.*, vol. 4, pp. 393–402, 2004.

[67] S. Kim and M. C. Miller, "Validation of a finite element humeroradial joint model of contact pressure using fuji pressure sensitive film," *J. Biomech. Eng.*, vol. 138, no. 1, 2016, doi: 10.1115/1.4031976.

[68] O. Lorbach *et al.*, "Medial Patellofemoral Ligament Reconstruction: Impact of Knee Flexion Angle During Graft Fixation on Dynamic Patellofemoral Contact Pressure—A Biomechanical Study," *Arthrosc. - J. Arthrosc. Relat. Surg.*, vol. 34, no. 4, pp. 1072–1082, 2018, doi: 10.1016/j.arthro.2017.09.047.

[69] M. G. Muriuki, L. G. Gilbertson, and C. D. Harner, "Characterization of the performance of a custom program for image processing of pressure sensitive film," *J. Biomech. Eng.*, vol. 131, no. 1, 2009, doi: 10.1115/1.3005150.

[70] G. A. Matricali, L. Labey, W. Bartels, G. Dereymaeker, F. P. Luyten, and J. Vander Sloten, "Repeatability and contact stress gradient detection of sealed pressure-sensitive film when used in a physiological joint model," *Proc. Inst. Mech. Eng. Part H J. Eng. Med.*, vol. 222, no. 7, pp. 1065–1071, 2008, doi:

10.1243/09544119JEIM389.

[71]   J. T. Finnoff *et al.*, "American Medical Society for Sports Medicine (AMSSM) Position Statement: Interventional Musculoskeletal Ultrasound in Sports Medicine," *PM R*, vol. 7, no. 2, pp. 151-168.e12, 2015, doi: 10.1016/j.pmrj.2015.01.003.

[72]   C. H. Turner and D. B. Burr, "Basic biomechanical measurements of bone: A tutorial," *Bone*, vol. 14, no. 4. pp. 595–608, 1993, doi: 10.1016/8756-3282(93)90081-K.

[73]   S. Wadugodapitiya, M. Sakamoto, K. Sugita, Y. Morise, M. Tanaka, and K. Kobayashi, "Ultrasound elastographic assessment of the stiffness of the anteromedial knee joint capsule at varying knee angles," *Biomed. Mater. Eng.*, vol. 30, no. 2, pp. 219–230, 2019, doi: 10.3233/BME-191046.

[74]   K. Hasegawa, "Elastic Properties of Osteoporotic Bone Measured by Scanning Acoustic Microscopy," *Bone*, vol. 16, no. 1, pp. 85–90, Jan. 1995, doi: 10.1016/s8756-3282(94)00013-1.

[75]   T. S. Tissues and C. Sciences, "The Soft Tissues in Osteoarthritis and Arthroplasty of the Hip Tarasevicius, Sarunas 2009," Lund University, 2009.

[76]   S. Kumaresan, N. Yoganandan, F. A. Pintar, D. J. Maiman, and S. Kuppa, "Biomechanical study of pediatric human cervical spine: A finite element approach," *J. Biomech. Eng.*, vol. 122, no. 1, pp. 60–71, 2000, doi: 10.1115/1.429628.

[77]   V. Lafage, N. Gangnet, J. Sénégas, F. Lavaste, and W. Skalli, "New interspinous implant evaluation using an in vitro biomechanical study combined   with a finite-element analysis.," *Spine (Phila. Pa. 1976).*, vol. 32, no. 16, pp. 1706–1713, Jul. 2007, doi: 10.1097/BRS.0b013e3180b9f429.

[78]   M. Arcan, Z. Hashin, and A. Voloshin, "A method to produce uniform plane-stress states with applications to fiber-reinforced materials," *Exp. Mech.*, vol. 18, no. 4, pp. 141–146, 1978, doi: 10.1007/BF02324146.

[79]   C. C. Lin, J. Da Li, T. W. Lu, M. Y. Kuo, C. C. Kuo, and H. C. Hsu, "A model-based tracking method for measuring 3D dynamic joint motion using an

alternating biplane x-ray imaging system," *Med. Phys.*, vol. 45, no. 8, pp. 3637–3649, Aug. 2018, doi: 10.1002/mp.13042.

[80] J. D. Mozingo *et al.*, "Validation of imaging-based quantification of glenohumeral joint kinematics using an unmodified clinical biplane fluoroscopy system," *J. Biomech.*, vol. 71, pp. 306–312, 2018, doi: 10.1016/j.jbiomech.2018.02.012.

[81] M. Hackl *et al.*, "Radial shortening osteotomy reduces radiocapitellar contact pressures while preserving valgus stability of the elbow," *Knee Surgery, Sport. Traumatol. Arthrosc.*, vol. 25, no. 7, pp. 2280–2288, 2017, doi: 10.1007/s00167-017-4468-z.

[82] P. Sun and X. Zhang, "Study on phase-shifting techniques in ESPI.," *Optoelectronics.Laser*, vol. 12, no. 11, pp. 1174–1176, 2001.

[83] P. Sun, X. Zhang, and H. Wang, "Study on combined method based on 3-D ESPI.," *Chinese J.Lasers*, vol. B11, no. 3, pp. 189–192, 2002.

[84] L. Wang, S. Bi, H. Li, Y. Gu, and C. Zhai, "Fast initial value estimation in digital image correlation for large rotation measurement," *Opt. Lasers Eng.*, vol. 127, p. 105838, Apr. 2020, doi: 10.1016/j.optlaseng.2019.105838.

[85] A. M. Felfelian, A. Baradaran Najar, R. Jafari Nedoushan, and H. Salehi, "Determining constitutive behavior of the brain tissue using digital image correlation and finite element modeling," *Biomech. Model. Mechanobiol.*, vol. 18, no. 6, pp. 1927–1945, 2019, doi: 10.1007/s10237-019-01186-6.

[86] W. H. Peters and W. F. Ranson, "Digital Imaging Techniques In Experimental Stress Analysis," *Opt. Eng.*, vol. 21, no. 3, pp. 427–431, Jun. 1982, doi: 10.1117/12.7972925.

[87] I. Yamaguchi, "A laser-speckle strain gauge," *J. Phys. E.*, vol. 14, no. 11, pp. 1270–1273, 1981, doi: 10.1088/0022-3735/14/11/012.

[88] J. Liu and R. Wang, "Shrinkage experimental study using digital image correlation method," *Rock Soil Mech.*, vol. 30, no. 6, pp. 1867–1872, 2009.

[89] P. F. Luo, Y. J. Chao, M. A. Sutton, and W. H. Peters, "Accurate measurement of three-dimensional deformations in deformable and rigid bodies using

computer vision," *Exp. Mech.*, vol. 33, no. 2, pp. 123–132, 1993, doi: 10.1007/BF02322488.

[90]   P.-F. Luo, Y. J. Chao, and M. A. Sutton, "Application of stereo vision to three-dimensional deformation analyses in fracture experiments," *Opt. Eng.*, vol. 33, no. 3, pp. 981–990, Mar. 1994, doi: 10.1117/12.160877.

[91]   Z. Tang and J. Liang, "Digital Image Correlation Method Based on Seed Point for Large Deformation Measurement," *J. Xi'an Jiaotong Univ.*, vol. 44, no. 11, pp. 51–55, 2010.

[92]   D. Zhang, C. D. Eggleton, and D. D. Arola, "Evaluating the mechanical behavior of arterial tissue using digital image correlation," *Exp. Mech.*, vol. 42, no. 4, pp. 409–416, 2002, doi: 10.1007/BF02412146.

[93]   M. L. Ruspi *et al.*, "Digital image correlation (DIC) assessment of the non-linear response of the anterior longitudinal ligament of the spine during flexion and extension," *Materials (Basel).*, vol. 13, no. 2, p. 384, Jan. 2020, doi: 10.3390/ma13020384.

[94]   B. Pan, K. Qian, H. Xie, and A. Asundi, "Two-dimensional digital image correlation for in-plane displacement and strain measurement: a review," *Meas. Sci. Technol.*, vol. 20, no. 6, p. 062001, Jun. 2009, doi: 10.1088/0957-0233/20/6/062001.

[95]   M. Palanca, G. Tozzi, and L. Cristofolini, "The use of digital image correlation in the biomechanical area: a review," *Int. Biomech.*, vol. 3, no. 1, pp. 1–21, Jan. 2016, doi: 10.1080/23335432.2015.1117395.

[96]   Y. Barranger, P. Doumalin, J. C. Dupré, and A. Germaneau, "Digital Image Correlation accuracy: influence of kind of speckle and recording setup," *EPJ Web Conf.*, vol. 6, p. 31002, Jun. 2010, doi: 10.1051/epjconf/20100631002.

[97]   M. Palanca, T. Brugo, and L. Cristofolini, "Use of digital image correlation to investigate the biomechanics of the vertebra," *J. Mech. Med. Biol.*, vol. 15, p. 1540004, Apr. 2015, doi: 10.1142/S0219519415400047.

Lebenslauf

Schulbildung

09/1997-07/2003   Dongfanghong Grundschule

09/2003-07/2006   Yueyang 4. Mittelschule

09/2006-07/2009   Yueyang 4. Oberschule

Studium

09/2009-07/2014   Nanhua Universität

                        Fach: Klinische Medizin

                        Abschlussziel: Bachelor

09/2015-07/2018   Hunan Normale Universität

                        Fach: Chirurgie

                        Abschlussziel: Master

04/2019-jetzt   Universität zu Köln

                        Fach: Humanmedizin

                        Abschlussziel: Dr.med

Arbeitserfahrungen

01/2013-01/2014   Hunan Volkskrankenhaus   Praktikantenärztin

09/2015-06/2018   Hunan Volkskrankenhaus   Praktikantenärztin

02/2019-03/2021   Uniklinik Köln   Forscherin